Title

THE K*p INTERACTION FROM 861+ to 1585 MeV/c; ANGULAR DISTRIBUTIONS FOR INELASTIC SCATTERING

Authors

Bland, R.W.
Bowler, M.G.
Brown, J.L.
et al.

Publication Date

1969-11-01

Submitted to Nuclear Physics B

UCRL-19357
Preprint

c.2

THE K^+p INTERACTION FROM 864 TO 1585 MeV/c; ANGULAR DISTRIBUTIONS FOR INELASTIC SCATTERING

R. W. Bland, M. G. Bowler, J. L. Brown, G. Goldhaber,
S. Goldhaber, J. A. Kadyk, V. H. Seeger, and G. H. Trilling

November 1969

AEC Contract No. W-7405-eng-48

LAWRENCE RADIATION LABORATORY
UNIVERSITY of CALIFORNIA BERKELEY

UCRL-19357

DISCLAIMER

UNIVERSITY OF CALIFORNIA

Lawrence Radiation Laboratory
Berkeley, California

April 14, 1970

ERRATA

TO: All recipients of UCRL-19357

FROM: Technical Information Division

SUBJECT: UCRL-19357, "The K^+p Interaction from 864 to 1585 MeV/c; Angular Distributions for Inelastic Scattering" by R. W. Bland, M. G. Bowler, J. L. Brown, G. Goldhaber, S. Goldhaber, J. A. Kadyk, V. H. Seeger, and G. H. Trilling

Please insert the attached pages in subject report.

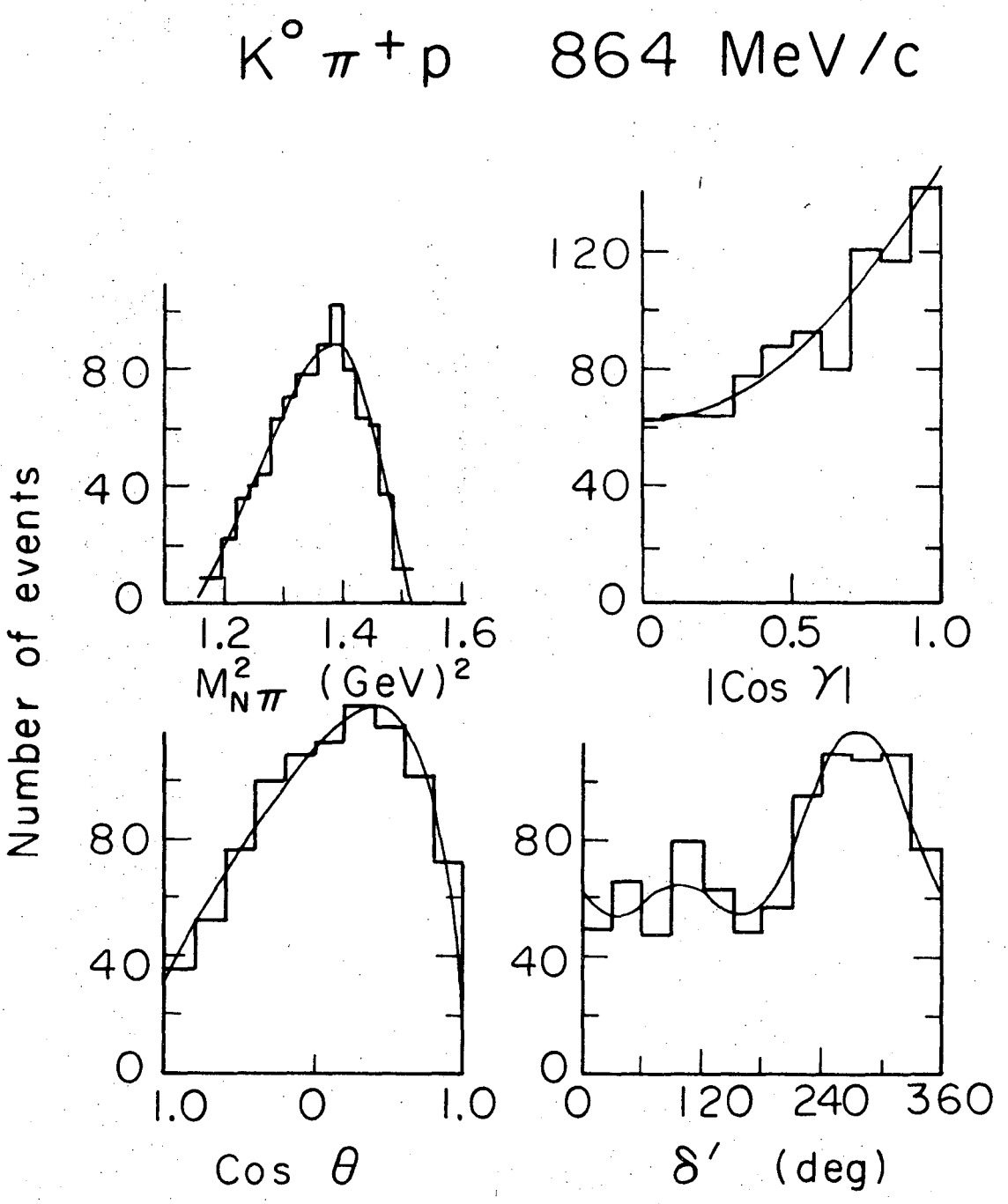
K° π+ p 864 MeV/c
Number of events
80
40
0
1.2
1.4
1.6
M²Nπ (GeV)²
120
80
40
0
0
0.5
1.0
|Cos γ|
80
40
0
1.0
0
1.0
Cos θ
80
40
0
0
120
240
360
δ′ (deg)
XBL6910-3902

Fig. 20a

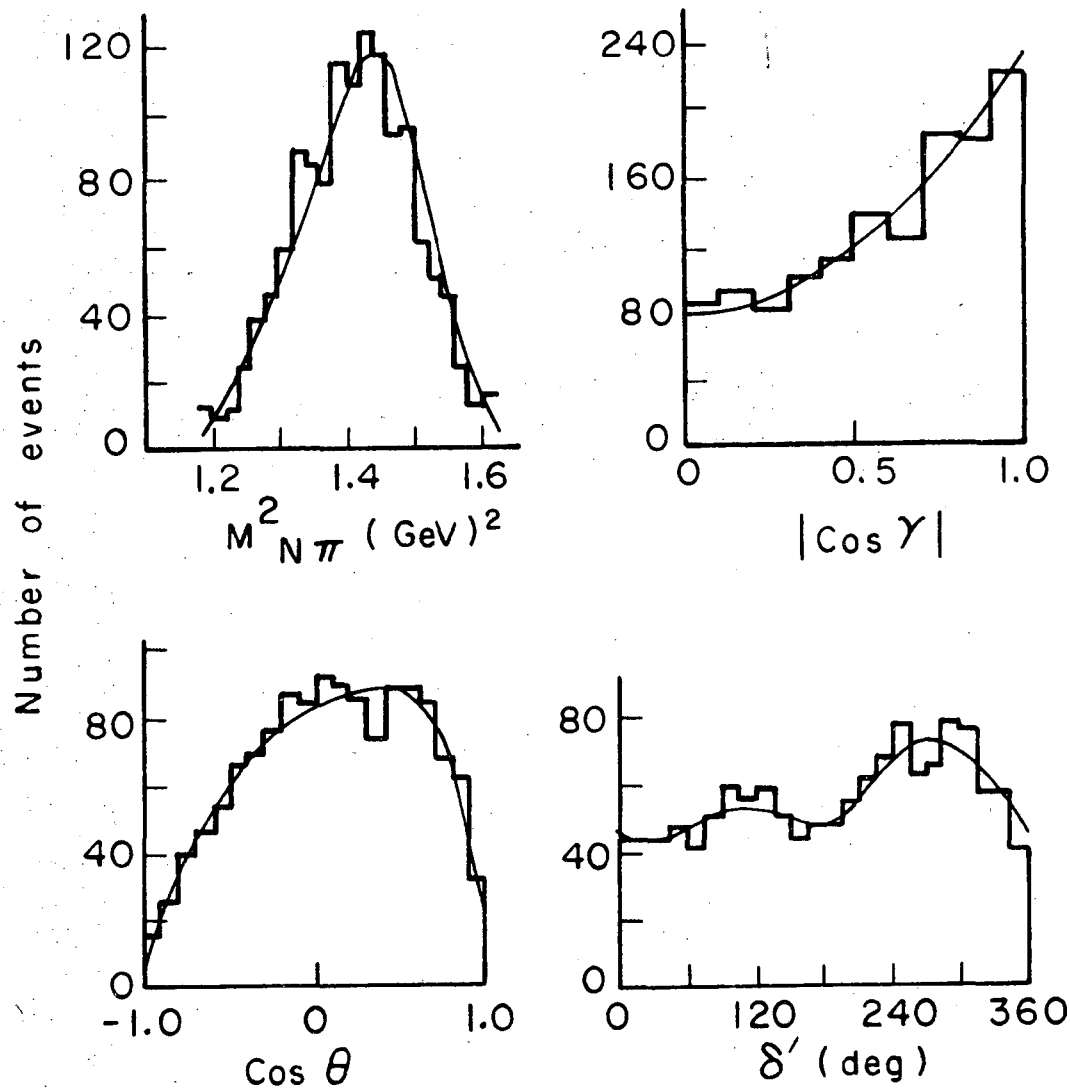
K°π⁺p 969 MeV/c
Number of events
120
80
40
0
1.2
1.4
1.6
M²Nπ (GeV)²
240
160
80
0
0
0.5
1.0
|Cos γ|
80
40
0
-1.0
0
1.0
Cos θ
80
40
0
0
120
240
360
δ′ (deg)
XBL6911-6193

Fig. 20b

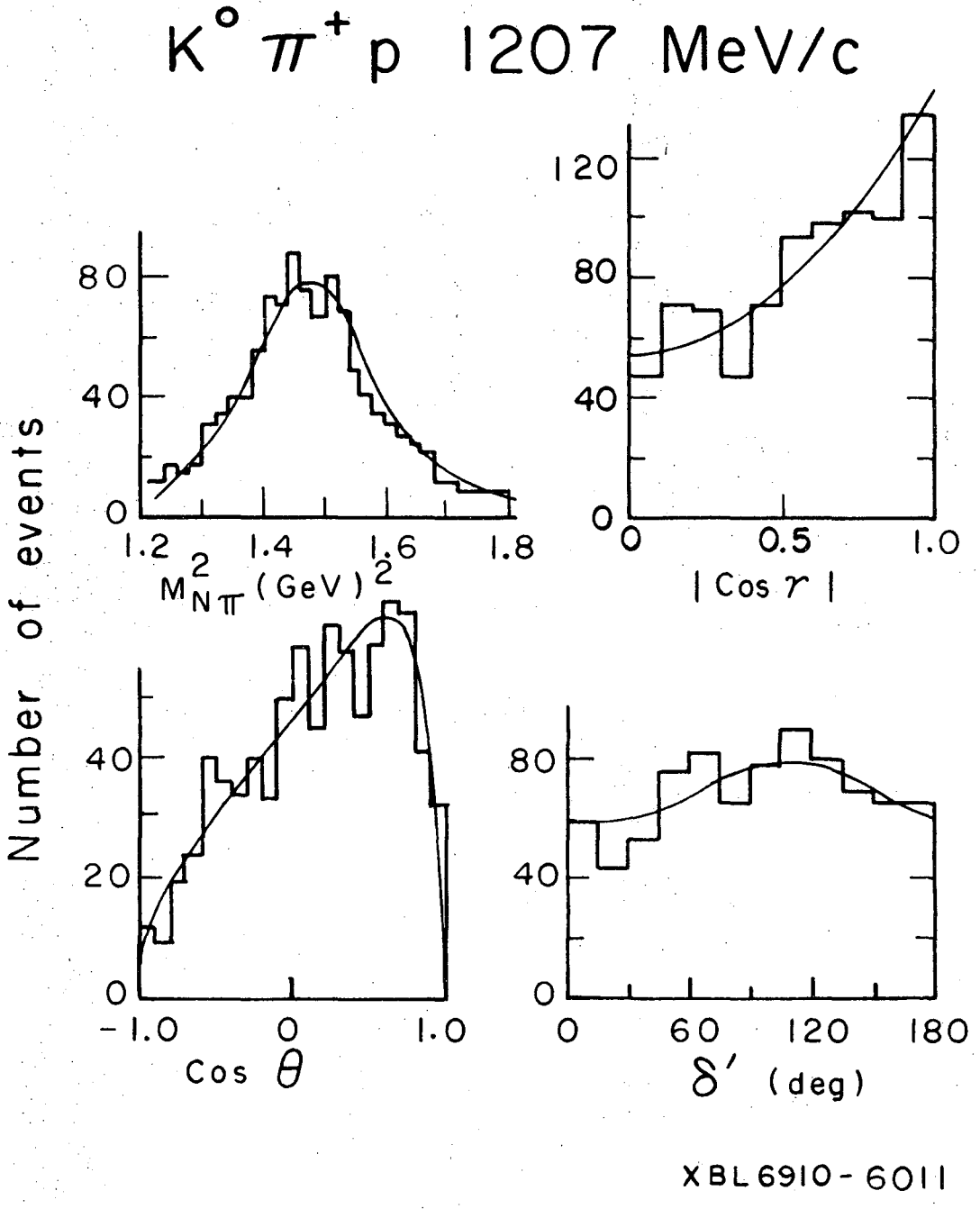
K° π⁺ p 1207 MeV/c
Number of events
80
40
0
1.2
1.4
1.6
1.8
$M^2_{N\pi}$ (GeV)^2
120
80
40
0
0
0.5
1.0
| Cos r |
40
20
0
-1.0
0
1.0
Cos θ
80
40
0
0
60
120
180
δ′ (deg)
XBL6910-6011

Fig. 20c

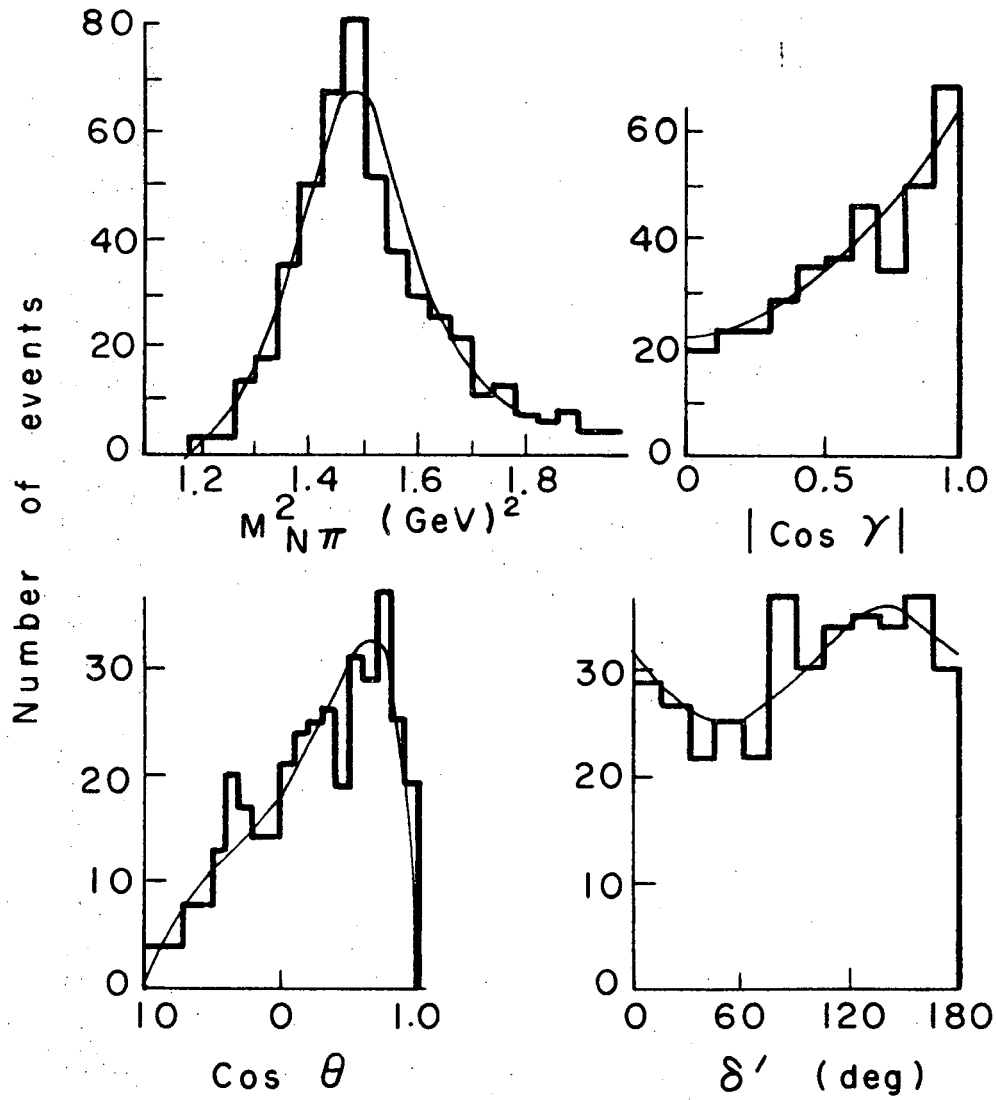
K°π⁺p 1367 MeV/c
Number of events
80
60
40
20
0
1.2
1.4
1.6
1.8
M²Nπ (GeV)²
60
40
20
0
0
0.5
1.0
|Cos γ|
30
20
10
0
10
0
1.0
Cos θ
30
20
10
0
0
60
120
180
δ′ (deg)
XBL610-3903

Fig. 20d

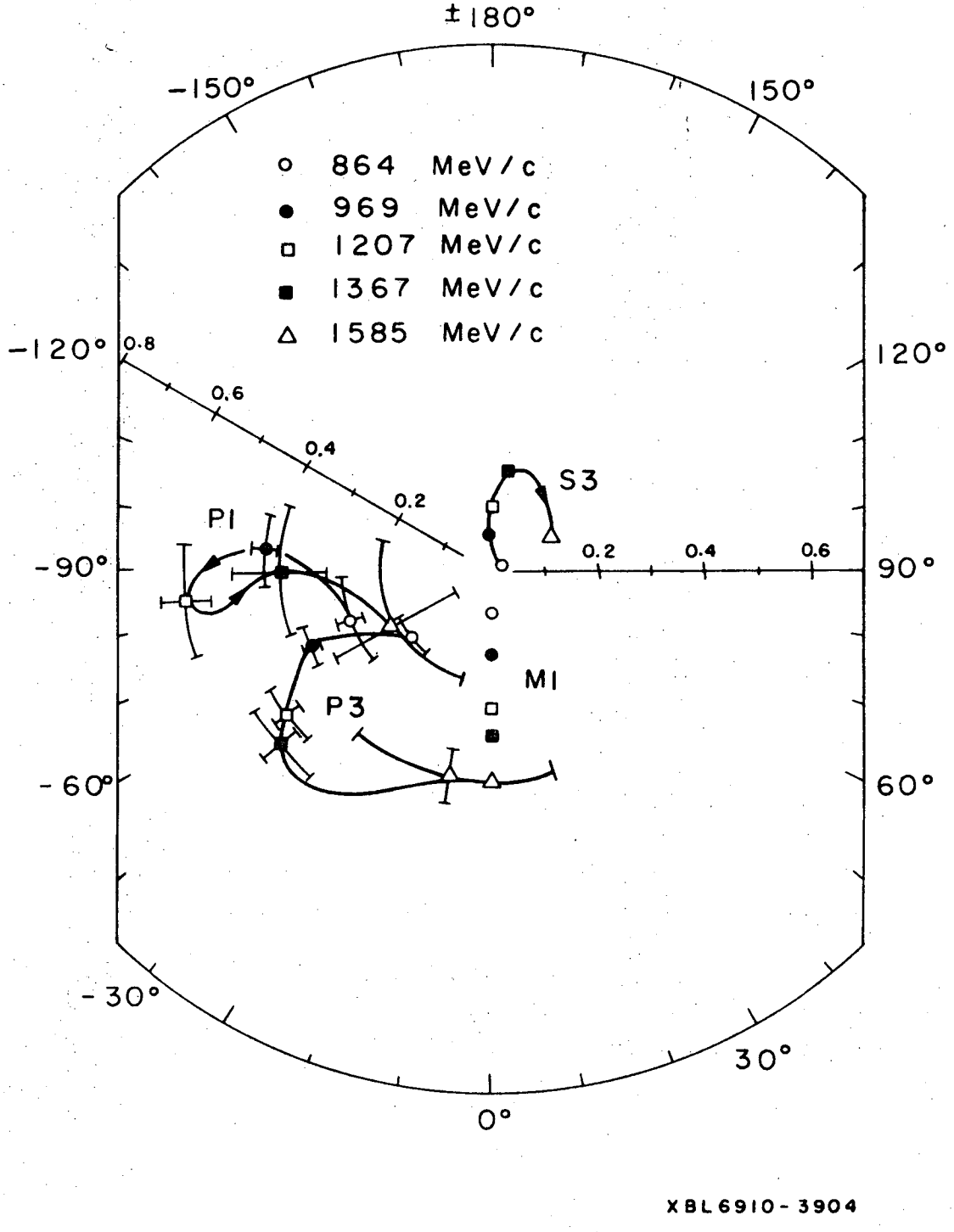
±180°
-150°
150°
-120°
120°
-90°
90°
-60°
60°
-30°
30°
0°
0.8
0.6
0.4
0.2
0.2
0.4
0.6
864 MeV/c
969 MeV/c
1207 MeV/c
1367 MeV/c
1585 MeV/c
P1
S3
M1
P3
XBL6910-3904

Fig. 21

THE K^+p INTERACTION FROM 864 TO 1585 MeV/c; ANGULAR DISTRIBUTIONS FOR INELASTIC SCATTERING

R. W. Bland,† M. G. Bowler,†† J. L. Brown,††† G. Goldhaber, S. Goldhaber,‡ J. A. Kadyk, V. H. Seeger, and G. H. Trilling

Department of Physics and Lawrence Radiation Laboratory
University of California, Berkeley, California 94720‡‡

November 1969

ABSTRACT

We present angular distributions for production and decay of the quasi-two-body final states $K\Delta(1236)$ and $K^*(891)p$ produced in K^+p interactions at 864, 969, 1207, 1367, and 1585 MeV/c. The analysis of these distributions leads to the following conclusions: (a) $K\Delta(1236)$ production near threshold is largely via P waves and is, except for coupling constants, fairly well approximated at all momenta by the predictions of the Stodolsky-Sakurai ρ-exchange model; (b) $K^*(891)p$ production appears dominated by vector exchange down to threshold, and no evidence of significant relative increase in pseudoscalar exchange contribution at low energy is seen; (c) study of the partial-wave structure of $K\Delta(1236)$ production shows no evidence of resonant behavior at the total cross section peak near 1200 MeV/c.

---

† Present address: Ecole Polytechnique, Paris
†† Present address: Nuclear Physics Laboratory, Oxford, England
††† Present address: Stanford Linear Accelerator Center, Stanford, California
‡ Deceased December 1965
‡‡ Work done under auspices of the U. S. Atomic Energy Commission

1. INTRODUCTION

In a previous paper[1] we have discussed cross sections and mass distributions for K^+p interactions from 864 to 1585 MeV/c. The dependence of the cross sections on momentum as discussed in that paper is shown in fig. 1. The total cross section peak is closely related to the sharp rise of the inelastic cross section. Single pion production dominates the inelastic cross section in the momentum region of our experiment, and consists almost entirely of $K^*(891)$ and $\Delta(1236)$ production. Thus, K^+p reactions below 1600 MeV/c are dominated by three (quasi-) two-body final states:

$$K^+p \rightarrow K^+p\,, \tag{1}$$

$$K^+p \rightarrow K\Delta(1236)\,, \tag{2}$$

$$\text{and} \quad K^+p \rightarrow K^*(891)p\,. \tag{3}$$

The small amount of double-pion production observed is also dominated by a quasi-two-body final state,

$$K^+p \rightarrow K^*(891)\Delta(1236)\,. \tag{4}$$

Reaction (1) has been discussed in a previous paper[2]; there is a smooth transition from low-energy isotropy to high-energy diffraction, with the diffractive behavior being well established by 1207 MeV/c. This paper will be devoted to the detailed characteristics of reactions (2)-(4).‡

2. EXPERIMENTAL ANGULAR DISTRIBUTIONS

Reactions (2) and (3) proceed through the three single-pion-production reactions,

$$K^+p \rightarrow K^0p\pi^+\,, \tag{5}$$

$$K^+p \rightarrow K^+p\pi^0\,, \tag{6}$$

‡Some further details on this experiment can be found in two unpublished theses, refs. 3) and 4). Numerical tabulations of much of the data are given in ref. 5).

and $K^+p \rightarrow K^+n\pi^+$. (7)

The K^+p system is pure I = 1, and it follows that the Δ and K^* are produced in reactions (5), (6), and (7) in the ratios 9:2:1 and 2:1:0, respectively. The $K^0p\pi^+$ final state [reaction (5)] is thus richest in resonance production, and will be emphasized in the ensuing discussion. The variables with which we describe the three-body final state are a diparticle effective mass, its production angle in the overall center-of-mass system, and a pair of decay angles in the diparticle center of mass. Since our data are dominated by Δ and K^* production, we will emphasize the $N\pi$ and $K\pi$ diparticle systems.

The mass cuts we use are given in Table 1. In addition to making these cuts, in the $K^0p\pi^+$ and $K^+p\pi^0$ final states at 1207, 1367, and 1585 MeV/c it is necessary to separate the Δ from the K^*. At 1207 and 1367 MeV/c the low-$K\pi$-mass half of the Dalitz plot is fairly free of K^* production. Therefore, at these momenta, we restrict ourselves to the region of the Dalitz plot corresponding to $\cos \lambda_{N\pi} > 0$, where $\lambda_{N\pi}$ is the decay angle defined in fig. 2. At 1585 MeV/c the K^* band lies in the center of the Dalitz plot, and a different method for purifying the Δ sample must be used. Applying the mass-conjugation technique of Eberhard and Pripstein[6], we use events in the upper part of the K^* band to simulate K^*- production events in the overlap region, and subtract them from the sample in the Δ band. This corrects for incoherent K^* production within the Δ band, but not for K^*-Δ interference, which we have ignored for the present purpose. We can estimate the amount of background in the resonance samples in the $K^0p\pi^+$ reaction by using the results of ref 1. For the Δ the background is about 20% at 864 MeV/c and $\lesssim$ 10% at the other four momenta. The background under the K^*, mainly due to the tail of the Δ, is about 40% at 1207 MeV/c, 15% at 1367 MeV/c, and 10% at 1585 MeV/c.

2.1 Δ(1236)-Production Angular Distributions

The production angular distribution for the KΔ final state is shown in fig. 3. We note two prominent features of the data: near threshold the distributions have a large $\sin^2\theta$ component; and, as the total c.m. energy increases, there is an increasing asymmetry toward the forward direction. The second feature continues smoothly into the high energy region, where the reaction is quite peripheral. A more quantitative description of these effects is given by the normalized Legendre coefficients, as defined by

$$W(\cos\theta) \propto 1 + \sum_{\ell=1} A_\ell P_\ell (\cos\theta). \qquad (8)$$

These coefficients are shown as a function of beam momentum in fig. 4, for our data and for other published data[7,8]. We have included for completeness coefficients for the $K^+\pi^0 p$ and $K^+\pi^+ n$ final states where available. They add little information about Δ production, however; differences from the $K^0\pi^+ p$ final state probably represent background effects.

Let us first consider the even Legendre coefficients. A_2 is large and negative near threshold, corresponding in the $\sin^2\theta$ character of the 864- and 969-MeV/c data. (Pure $\sin^2\theta$ corresponds to $A_2 = -1.$) The $\sin^2\theta$ component requires the presence of P or higher waves† in the final-state KΔ system, and it is remarkable that it is already strong at even the lowest momenta, where one might have expected that a final-state S wave would be favored by the absence of an angular momentum barrier factor. The A_4 coefficient is small near threshold, and becomes more significant with increasing momentum. The even coefficients thus show a large P-wave component near threshold, with a transition to higher waves taking place in the region of the cross-section peak.

---

†In discussing final states of the form $A+B^* \to A+C+D$ we use capital letters to denote the orbital A-B^* state and lower-case letters to denote the orbital C-D state.

The odd Legendre coefficients represent interference between waves of opposite parity, and should therefore reflect any rapid phase change in a single amplitude. From fig. 4 we see that both A_1 and A_3 are smooth and monotonic near 1200 MeV/c. This apparent lack of any rapid phase change is a crucial piece of evidence against a resonance in our partial-wave analysis of the KΔ final state, given in Sec. 4 below.

There is one further feature of the Δ-production angular distributions that is worth noting, although probably not relevant to the resonance question. This is displayed in fig. 5, where we show the two lowest Legendre coefficients as a function of the Nπ mass. Considering first the $K^o\pi^+p$ channel, we see that the forward-backward asymmetry A_1 varies dramatically with Nπ mass, and almost vanishes in the high-mass region. The second Legendre coefficient also varies markedly with mass. Such effects cannot result from Δ production alone, but must result from interference between the Δ and a background wave. The phase of the Δ relative to the background amplitudes then varies with Nπ mass as expected from the Δ Breit-Wigner dependence, giving the effect observed. The background amplitude must be of a rather special sort, however; since in the production angular distribution the decay angles in the Nπ c.m. have been integrated out, the interfering wave must have the Nπ system in a $p_{3/2}$ state, as other ℓ_j states are orthogonal to the $p_{3/2}$ Δ. Since the KΔ final state is almost entirely P-wave near threshold, the background wave must have components with both even K-(Nπ) orbital angular momentum, to produce the effect seen in the A_1 coefficient, and odd orbital angular momentum, to produce the effect in A_2. Comparison between the three charge states in fig. 5 provides some additional information. The change in the asymmetry coefficient A_1 with

increasing mass is large and negative for the $K^o\pi^+p$ final state. The effect is much weaker in the other two charge states, and a positive change with increasing mass is suggested in the $K^+\pi^op$ final state. We have not attempted to introduce into our analysis any background amplitude specifically designed to reproduce these effects.

2.2 Δ(1236) Decay Angular Distributions

We describe the decay of the Δ in a coordinate system in the Nπ c.m., with the x axis along the direction of the incoming proton as seen in the Nπ c.m., and the z axis along the direction of the normal to the production plane. The coordinate system and decay angles are illustrated in fig. 6; the decay angles refer to the nucleon from the Δ decay.

From symmetry considerations one can predict some properties of the decay angular distribution. First, the entire production and decay process is invariant under the parity transformation, or, equivalently, reflection about the Δ production plane. From fig. 6 we see that this corresponds to the transformation

$$\begin{Bmatrix} \cos\alpha \\ \phi \end{Bmatrix} \rightarrow \begin{Bmatrix} \cos\alpha \\ -\phi \end{Bmatrix} , \tag{9a}$$

or

$$\begin{Bmatrix} \cos\gamma \\ \delta \end{Bmatrix} \rightarrow \begin{Bmatrix} -\cos\gamma \\ \delta \end{Bmatrix} . \tag{9b}$$

We assume this symmetry in our analysis. A second symmetry is the parity inversion of the outgoing nucleon and pion in the Nπ c.m., corresponding to the transformation

$$\begin{Bmatrix} \cos\alpha \\ \phi \end{Bmatrix} \rightarrow \begin{Bmatrix} -\cos\alpha \\ \phi + \pi \end{Bmatrix} , \tag{10a}$$

or

$$\begin{Bmatrix} \cos\gamma \\ \delta \end{Bmatrix} \rightarrow \begin{Bmatrix} -\cos\gamma \\ \delta + \pi \end{Bmatrix} . \tag{10b}$$

This is a valid symmetry only if the Nπ system is in a state of definite parity. Interference between states of opposite parities introduces terms not satisfying this symmetry.

We have parameterized the decay angular distribution with the usual spin-3/2 density matrix elements [9]. To these we have added two functions satisfying Eq. (9a) which are odd under parity inversion of the Δ decay and thus represent interference of the Δ amplitude with a background amplitude. The motivation for these interference terms can be seen in the 864- and 969-MeV/c $K^o p\pi^+$ Dalitz plots (see ref. [1]), which exhibit a strong asymmetry favoring high Kπ mass. This asymmetry is conveniently expressed in terms of the decay angle $\lambda_{N\pi}$, defined in fig. 2, by noting that along a line of fixed $M^2_{N\pi}$, cos $\lambda_{N\pi}$ varies linearly with $M^2_{K\pi}$. We define the asymmetry between high and low Kπ mass as $A \equiv (H - L)/(H + L)$, where H is the number of events with cos $\lambda_{N\pi} < 0$ (high Kπ mass) and L is the number of events with cos $\lambda_{N\pi} > 0$ (low Kπ mass). In fig. 7 we show A for our data and for other published low-momentum data [7, 10]. The effect is quite significant and cannot be produced by Δ production and incoherent background, but is easily reproduced by interference between the Δ and a state of even orbital angular momentum in the Nπ system. Unfortunately, above the $K^*(891)$ threshold, the additional complexity of the Dalitz plot makes this type of interference almost impossible to establish. Consequently, fig. 7 shows A only for momenta below 1 GeV/c, and the interference terms R_1, R_2 in (11a) below are determined only for such momenta. The general form of the decay angular distribution including the interference terms is

$$W(\cos\alpha,\phi) = \frac{3}{4\pi}\left\{\rho_{33}\sin^2\alpha + \rho_{11}(1/3+\cos^2\alpha) - \frac{2}{\sqrt{3}}\,\mathrm{Re}\,\rho_{3,-1}\sin^2\alpha\cos 2\phi - \frac{2}{\sqrt{3}}\,\mathrm{Re}\,\rho_{3,1}\sin 2\alpha\cos\phi + R_1\cos\alpha + R_2\sin\alpha\cos\phi\right\}; \quad (11a)$$

or, in the (γ,δ) system,

$$W(\cos\gamma,\delta) = \frac{3}{4\pi}\left\{\rho'_{33}\sin^2\gamma + \rho'_{11}(1/3+\cos^2\gamma) - \frac{2}{\sqrt{3}}\,\mathrm{Re}\,\rho'_{3,-1}\sin^2\gamma\cos 2\delta + \frac{2}{\sqrt{3}}\,\mathrm{Im}\,\rho_{3,-1}\sin^2\gamma\sin 2\delta + R_1\sin\gamma\cos\delta + R_2\sin\gamma\sin\delta\right\}, \quad (11b)$$

where

$$\rho'_{33} \equiv \frac{1}{4}(3/2 - 2\rho_{33} - 2\sqrt{3}\,\mathrm{Re}\,\rho_{3,-1}),$$

$$\rho'_{11} + \rho'_{33} = \rho_{11} + \rho_{33} = 1/2$$

$$\frac{2}{\sqrt{3}}\,\mathrm{Re}\,\rho'_{3,-1} \equiv -1/4 + \rho_{33} - \frac{1}{\sqrt{3}}\,\mathrm{Re}\,\rho_{3,-1}, \quad (12)$$

$$\frac{2}{\sqrt{3}}\,\mathrm{Im}\,\rho'_{3,-1} \equiv -\frac{2}{\sqrt{3}}\,\mathrm{Re}\,\rho_{31},$$

and R_1, R_2 have the same definitions in either system.

We have determined the density matrix elements and the two interference parameters R_1 and R_2 by the maximum-likelihood technique. At those momenta where the crossing of the K^* band obscures part of the Δ band, we used data from restricted regions of the Dalitz plot, as described above.

Thus for momenta above K^* threshold, we were obliged to fold the angular distributions according to eq. (10) into the ranges $0 \leq (\cos \alpha, \cos \gamma) \leq 1$, $0 \leq (\phi, \delta) \leq \pi$, and as mentioned above to drop the interference terms R_1, R_2 from the expansions of eq. (11). At 864 and 969 MeV/c and in the $K^+\pi^+n$ final state at 1207 MeV/c, where no problems due to K^* production are encountered, the full expansion was used.

In fig. 8 we show the density matrix elements of eq. (11a) for the $K^o\pi^+p$ final state, as a function of beam momentum, and we give our corresponding cos γ and δ distributions in figs. 9 and 10, respectively. Results from other experiments[11-16] are included in fig. 8. In fig. 11 we show the variation of the density matrix elements with momentum transfer; this, along with the production angular distributions, provides in principle a complete description of the Δ production process. The behavior of all density matrix elements, as seen in fig 8, is smooth as a function of beam momentum, with no dramatic change near 1200 MeV/c. Thus neither in the production nor in the decay angular distributions do we see evidence for a resonance in the reaction $K^+p \rightarrow K\Delta$.

The interference-term coefficients R_1 and R_2 are given in table 2 for the $K^op\pi^+$ final state at 864 and 969 MeV/c. We give values for all events and for three regions of $M^2_{N\pi}$. The most striking feature is the variation of R_2 with Nπ mass. This is to be expected from a Δ-background interference, since the Δ amplitude changes phase rapidly with Nπ mass. We conclude that there is a coherent background amplitude with even Nπ orbital angular momentum. Furthermore, this amplitude cannot produce the interference effects seen in the production angular distribution, since the interference term it produces vanishes when integrated over Nπ c.m. decay angles.

From the discussions above, we find that the nonresonant background in the single-pion-production channel includes coherent components with the following properties:

a) $\ell_j = p_{3/2}$ for the $N\pi$ system, and even K-($N\pi$) orbital angular momentum [variation of A_1 with $M^2(N\pi)$];

b) $\ell_j = p_{3/2}$ for the $N\pi$ system and odd K-($N\pi$) orbital angular momentum [variation of A_2 with $M^2(N\pi)$];

c) even ℓ for the $N\pi$ system (variation in R_2).

Aside from the aforementioned interference effects, we can summarize the $K\Delta(1236)$ angular distribution as follows: The production angular distributions indicate the presence of large P waves at threshold, with higher waves coming in smoothly with momentum and with all odd Legendre coefficients increasing monotonically with momentum. The decay angular distributions show no marked change with momentum, and deviate only slightly from the magnetic dipole ρ-exchange predictions.

2.3 The $K^*(891)$ p Final State

We restrict our K^* sample to be in that half of the Dalitz plot away from the Δ ($\cos \lambda_{K\pi} < 0$), within the $K\pi$ mass band 840 — 940 MeV. This still does not give complete separation from the Δ at 1207 and 1367 MeV/c, but no more restrictive cuts can be made without biasing the angular distributions in a very complicated way. We find that results using a narrower $K\pi$ mass band, 870 — 910 MeV, are not distinguishable within statistical errors from those given here. We will consider events only from the $K^o\pi^+p$ final state. Besides our own data we include for comparison the data of Bettini et al. at 1450 MeV/c[8] and S. Goldhaber et al. at 1960 MeV/c[11].

The production angular distributions are given in fig. 12, and the corresponding Legendre coefficients in fig. 13. The variation in all the Legendre coefficients with momentum is remarkably smooth, with the reaction becoming steadily more peripheral with increasing momentum. We describe the decay of the K^* in a coordinate system similar to that used for the Δ (fig. 6); the z axis is along the normal to the production plane and the x axis is along the direction of the incoming K^+ meson as seen in the $K\pi$ c.m. The K^* decay angular distribution is given in terms of the density matrix elements as[9]

$$W(\cos\alpha, \phi) = \frac{3}{4\pi} \left\{ \rho_{00} \cos^2\alpha + \rho_{11} \sin^2\alpha - \rho_{1,-1} \sin^2\alpha \cos 2\phi \right.$$
$$\left. - \sqrt{2}\, \mathrm{Re}\, \rho_{10} \sin 2\alpha \cos\phi \right\}, \qquad (13)$$

where $\rho_{11} = \frac{1}{2}(1 - \rho_{00})$. In fig. 14 we show these density matrix elements as a function of momentum, and in fig. 15 the distributions in $\cos\alpha$ and ϕ are given. The curves correspond to the density matrix elements of fig. 14. There is evidently little change in the K^* alignment in this momentum region. The implications of these data in terms of exchange models are discussed in Sec. 3.

2.4 The $K^*(891)\ \Delta(1236)$ Final State

As discussed in ref. [1], K^+p double pion production near threshold is dominated by the $K^*\Delta$ final state. The major decay modes are produced in the reaction

$$K^+p \rightarrow K^+p\pi^+\pi^-. \qquad (14)$$

There is furthermore no ambiguity in this final state in pairing the particles. We discuss the $K^*\Delta$ final state only in reaction (14). In ref. 1 and $K^*\Delta$ final state was shown to constitute $65 \pm 15\%$ of reaction (14) at 1585 MeV/c; at 1367 Mev/c resonance production could not be separated from background.

In fig. 16 we show the $K^*\Delta$ c.m. production angular distributions, for our data and for those of Chinowsky et al.[17] at 1.96 GeV/c. (The 1.96-GeV/c data are restricted to events with the $p\pi^+$ and $K^+\pi^-$ masses in the Δ and K^* bands; ours have no such cut applied.) The reaction is remarkably forward-peaked, even at threshold.

The K^* and Δ density matrix elements [see eqs. (11) and (13)] are given in Table 3, along with those from Chinowsky et al.[17] at 1.96 GeV/c and Ferro-Luzzi et al.[18] at 3 GeV/c. The predictions for single-pion exchange are also given. While the higher-momentum data are roughly consistent with single-pion exchange, our data show substantially less alignment of the K^* and Δ than predicted.

We have tried to purify the double-resonance-production sample at 1585 MeV/c by considering only events with $M_{K\pi} > 800$ MeV, a cut which should have reduced the background from 35% to about 10%. No significant change was seen either in the production or decay angular distributions. Furthermore, cutting out nonperipheral events ($\cos\theta < 0.7$) also made no appreciable change in the angular distributions.

We conclude that even at threshold, $K^*\Delta$ production exhibits the beginnings of the peripheral character found at higher energy that is associated with one-pion exchange. The decay angular distributions in this experiment indicate less alignment than expected from a naive application of the O.P.E. mechanism, but evidently the alignment increases very rapidly with incident energy, since at 1.96 GeV/c, barely 400 MeV/c above threshold, the matrix elements have already taken on the values from which they deviate little at all higher energies that have been studied.

3. EXCHANGE MODEL DESCRIPTION OF KΔ AND K^*N PRODUCTION

One-particle-exchange models, modified by absorption corrections, Reggeization of the exchanged systems, or a combination of these, have had some success in accounting for many of the gross features of inelastic quasi-two-body processes at high energies. Thus KΔ, K^*N, $K^*\Delta$ production in high energy K^+p interactions have commonly been interpreted in terms, respectively, of ρ exchange, ω and π exchange, and pure π exchange. A remarkable aspect of these processes, indicated by the results of the preceding section, is that the features particularly characteristic of t-channel exchanges, namely peripheralism and particular alignment of the outgoing particles, seem to persist right down to threshold. It is this observation which we take as justification for making some qualitative comparisons between our data and exchange models in spite of the fact that our incident energies are really too low to expect such models to have validity.

3.1 Δ(1236) Production

The meson-exchange diagram for Δ production is shown in fig. 17. The exchanged particle must have I = 1, with normal spin-parity: $J^P = 0^+, 1^-, 2^+, \ldots$. Stodolsky and Sakurai proposed several years ago that the exchanged particle be a ρ meson and assumed magnetic dipole (M1) coupling to the Δ-p vertex[19]. The corresponding cross section[3] is given by

$$\frac{d^2\sigma}{d\cos\theta\, d\Omega_{decay}} = \frac{q'}{3\, sqm_\Delta^2} \frac{g_1^2}{4\pi} \frac{g_2^2}{4\pi} \left[\frac{E_p + m_p}{2m_\Delta} \frac{S}{(m_\rho^2 - t)^2}\right] \left\{\frac{1 + 3\cos^2\gamma}{2}\right\}, \tag{15}$$

where

q, q' are the c.m. momenta for the incoming and outgoing two-body systems,

s, t are the usual Mandelstam variables,

$S \equiv sq^2q'^2 \sin^2\theta$,

E_p = target proton total energy in the Δ rest system.

The basic predictions by the model are as follows:

$$W(\cos\gamma) = 1 + 3\cos^2\gamma, \tag{16a}$$

$$W(\delta) = \text{constant}, \tag{16b}$$

$$W(\cos\theta) = \frac{\sin^2\theta}{(m_\rho^2 - t)^2} \approx \frac{\sin^2\theta}{(1 - b\cos\theta)^2}, \tag{16c}$$

where $b = \dfrac{2qq'}{m_\rho^2 + 2\left(\sqrt{(q^2 + m_K^2)(q'^2 + m_K^2)} - m_K^2\right)}$.

Although eq. (15) assumes a zero-width Δ, we have, for purposes of calculation, multiplied by the Δ Breit-Wigner form [eq. (14) of ref. 1)] and integrated over the $N\pi$ mass.

The experimental cross section for the reaction $K^+p \to K\Delta$ is plotted in fig. 18. Curve (b) is the M1 prediction obtained by integrating eq. (15) over θ and γ. We have taken

$$\frac{g^2_{K^+\rho^+K^o}}{4\pi}\ \frac{g^2_{p\rho^+\Delta^{++}}}{4\pi} = 90\ , \tag{17}$$

as suggested by Jackson[9], and have multiplied the differential cross section by 4/3 so as to include all three final states, reactions (5), (6), and (7). The disagreement between experiment and theory is substantial.† We also show the prediction [(curve (a)] with the product of coupling constants, eq. (17), taken to be 450, which gives a good fit near threshold. This good agreement is, of course, just a consequence of the P-wave dominance of both the M1 model and the data at threshold. Since these coupling constants are determined by

†See ref. 26) of Bland thesis, ref. 3.

comparison between experiment and theory below 1 GeV/c, where the $K\Delta$ cross section is far below any unitarity limit, no absorption correction is necessary.

The production angular distributions predicted by the model are shown in fig. 3, together with our data. The agreement is fairly good; the model predicts largely P-wave production, as already suggested by our analysis of the $N\pi$ mass distributions in ref. 1. The predicted forward peaking is of course due to the presence of the ρ propagator, and the good agreement with experiment at the lower momenta confirms that the exchanged particle is a heavy one such as the ρ meson. At higher momenta the theory is not as peripheral as the data, a defect usually corrected by absorption or Reggeization.

We now examine the decay angular distributions. In terms of the density matrix elements, the magnetic dipole model predicts

$$\rho_{33} = 3/8 = 0.375$$

$$\text{Re } \rho_{3,-1} = \sqrt{3/8} = 0.218,$$

$$\text{Re } \rho_{31} = 0 .$$

In fig. 8 we see rather good agreement with the M1 predictions, from threshold to 12 GeV/c. The small discrepancies that do occur are primarily near threshold, where our data lie. In figs. 9 and 10 the predictions are compared with the experimental cos γ and δ distributions. The cos γ fits are rather good, but the details of the δ distribution are not reproduced by the model. In fig. 11 we show the experimental momentum-transfer dependence of the density matrix elements. The M1 model predicts no t-dependence for the density matrix elements, and in fact no consistent variation with t is evident in the data.

We can now make the following observations about the representation of the $K\Delta$ production in terms of a model such as the M1 ρ exchange model:

(a) The Δ spin-density matrix is well approximated by the predictions of the model at all energies from near threshold to the highest measured energies, above 12 GeV.

(b) At low energies the characteristic P-wave cross-section behavior and $\sin^2\theta$ production angular distribution predicted by the model are observed experimentally. At higher energies, the predictions of eq. (15) fail, as in fact they must to preserve unitarity, with the consequence that the KΔ cross section begins to fall rather than keep increasing as predicted, and the angular distribution is more peripheral than predicted, to a degree which becomes greater as the energy increases.

(c) In terms of present approaches to the description of KΔ production, it is highly likely that not only ρ but also A_2 exchange occurs. Thus the large values of the coupling constants are probably not too surprising.

It is not intended here to suggest that the magnetic dipole ρ exchange model is to be taken as correct in any literal sense, but rather to point out that eq. (15) is an approximately valid phenomenological representation of the observed low-energy KΔ production, with the choice of coupling constants given above. Comparison of our data with another version of the M1 model, the relativistic form of Jackson and Pilkuhn[9], is given in ref. 3.

3.2 K*(891) Production

It is already known that at higher energies the reaction $K^+p \to K^{*+}(891)p$ is dominated by the exchange of a normal spin-parity, isoscalar system, usually assumed to be the ω. Since the reaction $K^+n \to K^{*o}p$ is known, at higher energies, to be dominated by pion exchange[21], it follows from t-channel isospin considerations that some pion exchange is also present in the $K^+p \to K^{*+}p$

process. Indeed, phenomenological fits to experimental data in terms of combinations of pion and ω exchange have been made, with some success in representing production and decay angular distributions, but very little success in representing the energy dependence of the cross sections. Both absorptive and Regge exchange models predict that the ratio of pion to ω exchange should be largest at low energy and drop rapidly with increasing energy. If this behavior actually occurs, it should exhibit itself at the low energy of the present experiment by a much larger fraction of pion exchange relative to vector exchange than one finds at high energy.

If we use the usual angles α and ϕ, defined as polar and azimuthal angles with respect to the incident K^+ direction, as seen in the K^* rest system, pseudoscalar exchange leads to pure $\cos^2 \alpha$, corresponding to $\rho_{00} = 1$, and vector exchange to pure $\sin^2 \alpha$, with $\rho_{00} = 0$. From figs. 14 and 15, it is obvious that the data, even just 100 MeV/c above K^* threshold, exhibit dominance by vector exchange. In fact one can hardly establish any significant difference between the K^{*+} decay distributions at our lowest momentum and those at the highest energies that have been reported (12 GeV). In effect, pseudoscalar and pseudovector exchange appear to have essentially the same energy dependence, in disagreement with all exchange models. In view of this fundamental difference between observation and theoretical expectation, and because most of the phenomenological procedures for fitting theory and experiment are valid only at higher energies, it does not appear worthwhile to give in this paper any more detailed comparison between our data and existing theory. Such comparisons are discussed in ref 3.

4. PARTIAL-WAVE ANALYSIS OF THE KΔ FINAL STATE

The precise measurements of the total K^+p cross section by Cool et al.[22] and Bugg et al.[23] showed three structures, the most prominent being a bump of ≈ 4 mb at 1250 MeV/c. If this is a resonance, it is highly inelastic, with an implied elasticity of about 0.3 for a resonance fed by an incoming J = 1/2 wave, and less for higher-J waves. The KΔ final state is a promising candidate for the decay of such a resonance, as its cross section maximum occurs just above threshold, nearly under the total cross-section bump. In this section we examine the KΔ final state for evidence of resonant behavior.

Ideally in searching for a resonance in the KΔ channel one should perform a general partial-wave fit, using all low-order partial waves. However, without data on the final-state nucleon polarization, such a fit would be underconstrained. We can, however, do an analysis using a restricted set of waves which is still general enough to reproduce the main features of our data. As already noted, the distributions in Nπ mass and production angle suggest the dominance of P waves near threshold. As discussed in the preceding section, the magnetic dipole ρ-exchange model reproduces this feature and also fits the angular distributions fairly well. Our minimal set of partial waves should therefore include the lowest-order waves of the M1 model. To allow for complete freedom in the lower partial waves we include $P_{1/2}$ and $P_{3/2}$ waves, to be varied independently, and the amplitude M1', defined as the M1 amplitude with its $P_{1/2}$ and $P_{3/2}$ components subtracted out. This M1' amplitude represents our approximation to all partial waves higher than $P_{3/2}$. These three waves can reproduce most of the features of the $K^0\pi^+p$ final state. One feature not explained, however, is the apparent interference with a non-Δ background amplitude exhibited in fig. 7. We

therefore add the simplest background amplitude, s-wave in all particle pairs, which we call S1. (This wave is fed by the incident $P_{1/2}$ state, and has the same J^P as our P1 wave.) It interferes with the Δ amplitude to give the observed Dalitz plot asymmetry towards high $K\pi$ mass discussed in Section 1. Finally we include a $S_{3/2}$ $K\Delta$ final state, coming from an incident $D_{3/2}$ K^+p state. This wave is not important in our analysis, but we include it because of its a priori attractiveness as a possible candidate for a resonant state: the high inelasticity of the proposed resonance might be explained by the absence of an angular momentum barrier in the $S_{3/2}$ $K\Delta$ final state compared with the competing $D_{3/2}$ elastic final state.

The partial waves used in our analysis are given in table 4, with their corresponding angular distributions. We have also included in the table one other low-order partial wave, the $S_{1/2} \rightarrow D_{1/2}$ transition. The coordinate system in which we describe the decay of the $N\pi$ system is similar to that shown in fig. 6, but has as its x axis the direction of the incident K^+ as seen in the overall c.m. rather than the $N\pi$ rest system. The y axis is along the cross product of the production normal and the new x axis. We now use to describe the Δ decay the angles γ and δ', equivalent to the previously defined γ and δ except for the change in the x and y axes of the coordinate system.

Before carrying out a fit, we consider whether the peak in the $K\Delta$ cross section can arise from a single J^P state. If so, this might make a strong case for the existence of a Z^*, an S = 1 exotic baryon resonance, decaying predominantly into the $K\Delta$ final state. In fig. 19 we compare our data for reaction (2) at 969 MeV/c with the predictions for the various $K\Delta$ states given in table 4. We see that the only pure state consistent with the

cos θ and $|\cos \gamma|$ distributions is the $P_{3/2}$ state, while the δ' distribution rejects this hypothesis. The same features are present in our data at our other three momenta. It is thus clear that a superposition of waves is required to fit the data.

We have attempted to fit our data for reaction (5) separately at each momentum, using the five amplitudes; S1, S3, P1, P3, and M1'. The detailed forms of the amplitudes used and the parameterization of the energy dependence are given in ref. 3. The input information was the one-dimensional distributions in cos θ, cos γ, δ', and Nπ mass, with the sample selected as described in section 1.

No correlations were included, and in particular the variation of the angular distributions with Nπ mass was ignored. The δ' distribution was folded at 1207, 1367, and 1585 MeV/c, since the Δ sample was taken from only half of the Dalitz plot. The effect in the folded distributions of interference between Δ and background amplitudes is very difficult to calculate, and our analysis neglects this interference at 1207 MeV/c and higher momenta. Thus the S1 wave is treated as an incoherent phase-space-like background at these momenta.

The input data and fitted curves are given in figs 20 a-e. The fits are quite good. The cross-section contribution and phase for each partial wave are given in table 5. We have normalized the sum of the cross section contributions to the sum of the Δ production and background cross sections as given in ref. 1; contributions from K^* production and Δ-K^* interference are thus excluded. The corresponding partial-wave amplitudes are displayed in

fig 21.† The phases of the KΔ amplitudes are of course dependent on the Nπ mass. In fitting the data we have evaluated the phase at the mass corresponding to the peak of the Nπ mass distribution, as given in table 1, and we use that phase in fig. 21. Since one phase is arbitrary, we take the M1' amplitude to be real; it represents a ρ-exchange background which should not change phase rapidly. The amplitudes are normalized so that the unit circle on fig. 21 represents complete absorption of the appropriate incoming wave:

$$\sigma = \pi\lambda^2\left\{S1^2 + 2S3^2 + P1^2 + 2P3^2 + 2M1'^2\right\}. \qquad (29)$$

There is an ambiguity in the amplitudes determined by our fit due to the fact that only complex "dot products" of amplitudes appear in the calculations; all phases could be reversed in sign without changing the fit. The finite width of the Δ, however, allows us to resolve this ambiguity; since if we assume that the S1 background term has a fairly constant phase, the Δ background relative phase varies in a well-defined way with Nπ mass.

In fig. 21 a totally resonant amplitude would start at the center of the plot, traverse a counterclockwise circle with increasing energy, and return to the center. A resonant amplitude superimposed on a constant background would follow a circular trajectory which would not necessarily pass through the center. 969 and 1367 MeV/c are respectively about one half-width below and above the center of the peak in the total cross section as estimated by Cool et al., and span the peak in the Δ production cross section. One would thus expect a pure resonant amplitude to go through a phase change of about 90 deg between 969 and 1367 MeV/c. We see from

†The Argand plot given here differs from that in ref. 3 in the following respects: final data at 1585 MeV/c have somewhat changed the solutions at that momentum, and, due to a previous programming error, errors at the other momenta have been increased by a factor of $\sqrt{2}$.

fig. 21 that in fact the dominant P1 and P3 amplitudes are nearly stationary in this region, over a range in total c.m. energy of 170 MeV, and the S3 amplitude is always small. (The total c.m. energies corresponding to the five momenta analyzed are: 1730, 1780, 1890, 1960, and 2060 MeV.) Our analysis thus shows no substantial resonant component in any partial-wave amplitude in the region of the total cross-section peak.

A feature of the P3 trajectory in fig. 21 that must be noted is the large phase change between 1367 and 1585 MeV/c. This could indicate an uncompleted resonant trajectory, somewhat above the Cool peak and with a very large width. More probably it is due to the breakdown of the validity of the simple set of amplitudes that we have chosen. It is a deficiency of the M1 amplitude that it is less peripheral at higher energies than the data. Our fit at 1585 MeV/c is probably compensating for this deficiency in the M1' amplitude by maximizing the 2 P3·M1' term, which gives a forward asymmetry.

It is interesting to note from table 5 that the partial-wave solutions at the three lower momenta have P1 and P3 present in about a 1:1 cross-section ratio, instead of the 1:5 ratio predicted by the magnetic dipole model. It is this difference that accounts for the main deviations of the decay angular distributions from the magnetic dipole predictions.

To summarize the results of the partial-wave analysis, our simple model gives a good representation of the experimental data from 864 to 1367 MeV/c, throughout the region of the total cross-section peak. Δ production is dominated by the $P_{1/2}$ and $P_{3/2}$ states, in roughly equal amounts near threshold and in more nearly the magnetic dipole ratio of 1:5 at higher momenta. No rapid phase variation is seen in either of the dominant ampli-

tudes in the region of the total cross-section peak. Thus, although a small resonant component in either of the P waves cannot be ruled out, the 1200-MeV/c maximum in the Δ production cross section is clearly not due primarily to a single resonant amplitude.

5. SUMMARY

Since single pion production in the K^+p channel is strongly dominated by the KΔ and K^*N quasi-two-tody final states, with very little nonresonant background, our analysis has emphasized resonance production.

Most of our events can be attributed to the reaction $K^+p \rightarrow K\Delta$. This reaction shows the following features:

(a) The production near threshold is largely via P waves, as predicted by the magnetic dipole ρ-exchange model. This is indicated by the shape of the Nπ mass distribution, the rate of rise of the cross section with incident momentum, the strong $\sin^2\theta$ component in the production angular distribution, and the Δ alignment as determined by its decay angular distribution.

(b) The ρ-exchange squared coupling constants as determined near threshold are about five times as large as expected on theoretical grounds; and the cross section ratio for the $P_{1/2}$ and $P_{3/2}$ KΔ states, as determined from the decay angular distributions, is about 1:1 near threshold, instead of 1:5 as predicted by the M1 model.

(c) The Δ decay angular distributions vary little as a function of momentum, and are always fairly well approximated by the M1 predictions: $W(\cos\gamma) = 1 + 3\cos^2\gamma$, $W(\delta)$ = isotropic.

The K^* production is similar in may respects in the Δ production.

a) Near threshold the K^* is produced in low partial waves, with a rapidly rising cross section. The production angular distributions are consistent with vector exchange, which is largely P-wave near threshold.

b) The decay angular distributions are characteristic of vector exchange, with little change from threshold to the high-energy region. In particular, pseudoscalar exchange does not seem to become a more important part of the process even at threshold, in disagreement with expectations from either absorptive or Regge exchange models.

Even though t-channel exchange allows a qualitative explanation of all phenomena observed in the inelastic reactions, the interest in possible K^+p resonances has induced us to study the partial-wave structure of the inelastic reactions in more detail. Our partial-wave model for the $K\Delta$ final state has succeeded in fitting our data reasonably well in the region of the total cross-section bump, with no evidence at that energy for a resonance in the dominant P waves. This is presumably equivalent to the observation that the Legendre coefficients for the Δ production angular distribution and the density matrix elements are smooth functions of momentum. The latter is true for the K^*N final state, from its threshold just below the total cross-section maximum up to 2 GeV/c. It seems unlikely that a conventional resonance, with a rapid phase variation in the inelastic amplitude with total c.m. energy, could pass these tests undetected. These observations are in complete accord with the result of our previous analysis that the structure in the total cross section arises from the superposition of channel cross sections that are smooth but have widely separated thresholds[1]. It may be noted that phase-shift analyses of elastic K^+p scattering based both on angular distributions and on recent polarization measurements give $P_{3/2}$ and $P_{1/2}$

waves with positive and negative phases respectively[24]. The $P_{3/2}$ amplitude becomes increasingly absorptive as a function of incident momentum. Although it may be possible to interpret this behavior in terms of a very inelastic resonance, our data as discussed above do not give support to such an interpretation in the energy range studied here.

Table 1. Mass bands used in the analysis of Δ and K^* production, and the experimental peak positions of the $M^2_{N\pi}$ distributions (for cos $\lambda_{N\pi} > 0$ at 1207, 1367, and 1585 MeV/c).

Momentum (MeV/c)	$M^2_{N\pi}$ peak position $(GeV)^2$	Δ band $(GeV)^2$	K^* band (MeV)
864	$(1.170)^2$	no limits	-
969	$(1.191)^2$	no limits	-
1207	$(1.212)^2$	1.35—1.65	840—940
1367	$(1.212)^2$	1.35—1.65	840—940
1585	$(1.210)^2$	1.35—1.65	840—940

Table 2. Values of the interference-term coefficients R_1 and R_2 for the reaction $K^+p \rightarrow K^o p\pi^+$ at 864 and 969 MeV/c.

Momentum (MeV/c)	$M_{N\pi}$ region (GeV)	R_1	R_2
864	all events	0.08 ± 0.02	-0.13 ± 0.02
864	$M_{N\pi} < 1.32$	0.11 ± 0.03	-0.21 ± 0.03
864	$1.32 < M_{N\pi} < 1.40$	0.06 ± 0.03	-0.12 ± 0.03
864	$M_{N\pi} > 1.40$	0.06 ± 0.03	-0.06 ± 0.03
969	all events	0.033 ± 0.014	-0.066 ± 0.014
969	$M_{N\pi} < 1.36$	0.05 ± 0.03	-0.17 ± 0.03
969	$1.36 < M_{N\pi} < 1.45$	0.06 ± 0.02	-0.08 ± 0.02
969	$M_{N\pi} > 1.45$	-0.01 ± 0.02	0.03 ± 0.02

Table 3. K^* and Δ density matrix elements for the reaction $K^+p \to K^{*o}\Delta^{++} \to K^+p\pi^+\pi^-$.

	K^*			Δ		
Momentum (GeV/c)	ρ_{00}	$\rho_{1,-1}$	$Re\rho_{10}$	ρ_{33}	$Re\ \rho_{3,-1}$	$Re\ \rho_{31}$
1.367	0.23 ± 0.10	-0.14 ± 0.10	-0.01 ± 0.06	0.12 ± 0.08	0.17 ± 0.06	0.04 ± 0.07
1.585	0.43 ± 0.06	-0.01 ± 0.05	-0.06 ± 0.04	0.23 ± 0.04	-0.04 ± 0.04	0.02 ± 0.05
1.96[a]	≈ 0.8			≈ 0.12		
3.0[b]	0.76 ± 0.05	-0.03 ± 0.03	-0.13 ± 0.02	0.01 ± 0.04	-0.035 ± 0.035	0.07 ± 0.02
Predictions for pion exchange	1	0	0	0	0	0

a. We give approximate values deduced from angular distributions given in ref. 17.

b. Reference 18.

Table 4. Low-order partial waves for the reaction $K^+p \to K\Delta$ and their corresponding distributions in Δ production and decay angles.

K^+p initial state	$K\Delta$ final state	J^P	Name	Production angular distribution	Decay angular distributions $\cos\gamma$	Decay angular distributions δ'
$D_{3/2}$	$S_{3/2}$	$3/2^-$	S3	Isotropic	$1-\frac{3}{5}\cos^2\gamma$	$1+\frac{1}{2}\cos 2\delta'$
$P_{1/2}$	$P_{1/2}$	$1/2^+$	P1	Isotropic	$1-\frac{3}{5}\cos^2\gamma$	$1+\frac{1}{6}\cos 2\delta'$
$P_{3/2}$	$P_{3/2}$	$3/2^+$	P3	$1-\frac{4}{5}P_2(\cos\theta)$	$1+\frac{21}{13}\cos^2\gamma$	$1+\frac{11}{30}\cos 2\delta'$
$S_{1/2}$	$D_{1/2}$	$1/2^-$	D1	Isotropic	$1-\frac{3}{5}\cos^2\gamma$	$1-\frac{1}{6}\cos 2\delta'$
$P_{1/2}$	----	$1/2^+$	S1	Isotropic	Isotropic	Isotropic
			M1'		$1+3\cos^2\gamma$	Isotropic

UCRL-19357

Table 5. Partial-wave solutions for the $K^{o}\pi^{+}p$ final state; each double entry gives the cross-section contribution and the phase, relative to the M1' amplitude.

Momentum (MeV/c)	$\pi\lambda^2$ (mb)	Cross section (mb), phase (deg) S1 (background)	S3	P1	P3	M1'	Sum
864	5.6	0.20 ± 0.06 43 ± 15	0.01 ± 0.01 120 ± 55	0.44 ± 0.06 -70 ± 17	0.42 ± 0.05 -51 ± 13	0.08 ± 0.03 0	1.15
969	4.7	0.12 ± 0.07 18 ± 27	0.04 ± 0.06 -175 ± 17	0.88 ± 0.10 -95±9	1.28 ± 0.10 -68±6	0.25 ± 0.06 0	2.57
1207	3.4	0.41 ± 0.16 ---	0.11 ± 0.11 178 ± 17	1.17 ± 0.18 -84 ± 11	1.51 ± 0.16 -54 ± 7	0.47 ± 0.08 0	3.68
1367	2.9	0.23 ± 0.14 ---	0.22 ± 0.10 170 ± 22	0.47 ± 0.21 -89 ± 18	1.56 ± 0.23 -50 ± 9	0.55 ± 0.08 0	3.05
1585	2.3	0.59 ± 0.11 ---	0.08 ± 0.16 120 ± 50	0.10 ± 0.13 -62 ± 45	0.75 ± 0.20 -12 ± 27	0.73 ± .10 0	2.30

FIGURE CAPTIONS

Fig. 1. The K^+p partial and total cross sections as functions of beam momentum, as given in Ref. 1.

Fig. 2. Definition of $\lambda_{N\pi}$, the pion decay angle in the $N\pi$ c.m. with respect to the direction of the outgoing kaon.

Fig. 3. Differential cross section for $K^+p \to K^o\Delta^{++}$, at our five momenta. Left-hand scales on each figure refer to $d\sigma/d\Omega$ in mb/sr; right-hand scales refer to $d\sigma/dt$ in $mb/(GeV/c)^2$. The transformation from $\cos\theta$ to t is approximate, assuming the Δ peak mass values given in Table 1. The distributions include some background, and so do not integrate exactly to the Δ-production cross sections given in Ref. 1.

Fig. 4. Coefficients in the Legendre expansion of the $K\Delta$ production angular distribution, $d\sigma/d\Omega \propto 1 + \sum_{\ell=1} A_\ell P_\ell (\cos\theta)$. The curves are the predictions of the M1 ρ-exchange model, described in Sec. 2, normalized at each momentum to the number of events on the graph.

Fig. 5. Variation of the $K\Delta$ Legendre coefficients with $M^2_{N\pi}$.

Fig. 6. Coordinate system used in describing the Δ decay. The decay angles refer to the direction of the decay nucleon. Here $\hat{n} = p_{K\text{-in}} \times p_{K\text{-out}} / |p_{K\text{-in}} \times p_{K\text{-out}}|$.

Fig. 7. The $KN\pi$ Dalitz plot asymmetry coefficient A as a function of beam momentum.

Fig. 8. Density matrix elements for the Δ produced in the reaction $K^+p \to K^o\Delta^{++}$. The magnetic dipole model predicts $\rho_{33} = 0.375$, Re $\rho_{3,-1} = 0.218$, and Re $\rho_{3,1} = 0$.

Fig. 9. Distribution in cos γ for the Δ^{++} decay at our five momenta. Assuming overall parity conservation, we have folded the distributions about cos $\gamma = 0$. The curves show the predictions of the magnetic dipole model, $W(\cos \gamma) \propto 1 + 3 \cos^2 \gamma$.

Fig. 10. Distributions in δ for the Δ^{++} decay at our five momenta. At 864 and 969 MeV/c the distributions cover the full range $0 < \delta < 2\pi$; the background-interference effect is seen in the $\sin \delta$ component. At higher momenta where the K* is present we show distributions in $\delta_{\text{mod } \pi}$. The magnetic-dipole model predicts isotropy in δ, as shown by the solid lines.

Fig. 11. Density matrix elements for Δ decay as a function of the momentum transfer squared t.

Fig. 12. Differential cross section for $K^+p \to K^* + p$.

Fig. 13. Normalized Legendre coefficients for the K^* production angular distribution, as a function of beam momentum; $d\sigma/d\Omega \propto 1 + \sum_{\ell=1} A_\ell P_\ell(\cos \theta)$.

Fig. 14. Density matrix elements for K^* production in the reaction $K^+p \to K^{*+}p$, $K^{*+} \to K^o\pi^+$, as a function of beam momentum. Here $|t|$ is in $(\text{GeV/c})^2$.

Fig. 15. K^* decay angular distributions for the reaction $K^+p \to K^*p$, $K^* \to K^o\pi^+$. The curves correspond to the density matrix elements given in fig. 14.

Fig. 16. Production angular distribution for $K^+p \to K^*\Delta$.

Fig. 17. Feynman diagram for Δ production by ρ exchange.

Fig. 18. Experimental cross sections for $K^+p \to K\Delta$ as a function of beam momentum, and the predictions of ρ exchange with M1 coupling. Curve

(a) represents M1, $(g^2_{K^+\rho^+K^o}/4\pi)\,(g^2_{p\rho^+\Delta^{++}}/4\pi) = 450$. Curve (b) represents M1, $(g^2_{K^+\rho^+K^o}/4\pi)(g^2_{p\rho^+\Delta^{++}}/4\pi) = 90$.

Fig. 19. $N\pi$ production and decay angular distributions for the reaction $K^+P \rightarrow K^o p\pi^+$ at 969 MeV/c, and the predictions for production in various low-order partial waves.

Fig. 20. $N\pi$ mass distributions and Δ production and decay angular distributions used as input to the partial wave analysis of the $K\Delta$ final state, and the curves corresponding to the partial wave solutions. (a) for 864 MeV/c; $\chi^2 = 35$ for 40 d.o.f. (b) For 969 MeV/c; $\chi^2 = 64$ for 68 d.o.f. (c) For 1207 MeV/c; $\chi^2 = 75$ for 62 d.o.f. (d) For 1367 MeV/c; $\chi^2 = 41$ for 50 d.o.f. (e) For 1585 MeV/c; $\chi^2 = 55$ for 43 d.o.f.

Fig. 21. Argand diagram for $K^+p \rightarrow K\Delta$. See text for details.

REFERENCES

1. R. W. Bland, M. G. Bowler, J. L. Brown, G. Goldhaber, J. A. Kadyk, S. Goldhaber, V. H. Seeger, and G. H. Trilling, Nucl. Physics B13 (1969) 595.
2. R. W. Bland, G. Goldhaber, and G. H. Trillings, Phys. Letters 29B (1969) 618.
3. R. W. Bland (Ph. D. Thesis), Lawrence Radiation Laboratory Report UCRL-18131, March 1968 (unpublished)
4. V. H. Seeger (Ph. D. Thesis), Lawrence Radiation Laboratory Report (in preparation).
5. Trilling-Goldhaber Group Memo TG-170, Lawrence Radiation Laboratory, Berkeley, California (unpublished).
6. P. Eberhard and M. Pripstein, Phys. Rev. Letters 10 (1963) 351
7. T. A. Filippas, V. P. Henri, B. Jongejans, M. Krammer, J. M. Perreau, S. Focardi, A. Minguzzi-Ranzi, L. Monari, G. Saltini, P. Serra, E. Barralet, E. Huffer, and F. Muller, Nuovo Cimento 51A (1967) 1053.
8. A. Bettini, M. Cresti, S. Limentani, L. Perruzzo, R. Santangelo, D. Locke, D. J. Crennell, W. T. Davies, and P. B. Jones, Physics Letters 16, (1965) 83; G. B. Chadwick, D. J. Crennell, W. T. Davies, M. Derrick, J. H. Mulvey, P. B. Jones, D. Radojicic, C. A. Wilkinson, A. Bettini, M. Cresti, S. Limentani, L. Perruzo, and R. Santangelo, Physics Letters 6 (1963) 309.
9. J. D. Jackson and H. Pilkuhn, Nuovo Cimento 33 (1964) 906; 34 (1964) 1841E.

10. J. Fisk, H. K. Ticho, D. H. Stork, W. Chinowsky, G. Goldhaber, S. Goldhaber, and T. F. Stubbs, in Proceedings of the 1962 International Conference on High-Energy Physics at CERN, J. Prentki, editor (CERN, Geneva 23, Switzerland).

11. S. Goldhaber, W. Chinowsky, G. Goldhaber, and T. O'Halloran, Phys. Rev. 142 (1966) 913.

12. F. Bomse, S. Borenstein, J. Cole, D. Gillespie, R. Kraemer, B. Luste, I. Miller, E. Moses, A. Pevsner, R. Singh, and R. Zdanis, Phys. Rev. 158, (1967) 1298.

13. M. Ferro-Luzzi, R. George, Y. Goldschmidt-Clermont, V. P. Henri, B. Jongejans, D. W. G. Leith, G. R. Lynch, F. Muller, and J. -M. Perreau, Nuovo Cimento 36 (1965) 1101.

14. Chumin Fu, Lawrence Radiation Laboratory Report UCRL-18417, Aug. 1968 (unpublished).

15. V. G. Lind, G. Alexander, A. Firestone, C. Fu, and G. Goldhaber, Nuclear Physics B14 (1969) 1.

16. J. C. Berlinghieri, M. S. Farber, T. Ferbel, B. E. Forman, P.F. Slattery, and H. Yuta, Nuclear Physics B8 (1968) 333.

17. W. Chinowsky, G. Goldhaber, S. Goldhaber, W. Lee, and T. O'Halloran, Phys. Rev. Letters 9 (1962) 330.

18. M. Ferro-Luzzi, R. George, Y. Goldschmidt-Clermont, V. P. Henri, B. Jongejans, D. W. G. Leith, G. R. Lynch, F. Muller, and J. -M. Perreau, Nuovo Cimento 39 (1965) 417.

19. L. Stodolsky and J. J. Sakurai, Phys. Rev. Letters 11, (1963) 90; the first evidence for vector exchange was presented by S. Goldhaber [S. Goldhaber, W. Chinowsky, G. Goldhaber, and T. O' Halloran, Bull. Am. Phys. Soc. 8 (1963) 20] at the American Physical Society Meeting in New York, January 1963.

20. G. Goldhaber, W. Chinowsky, S. Goldhaber, W. Lee, and T. O' Halloran, Physics Letters 6 (1963) 62.

21. S. Goldhaber, J. L. Brown, I. Butterworth, G. Goldhaber, A. A. Hirata, J. A. Kadyk, and G. H. Trilling, Phys. Rev. Letters 15 (1965) 737.

22. R. L. Cool, G. Giacomelli, T. F. Kycia, B. A. Leontic, K. K. Li, A. Lundby, and J. Teiger, Phys. Rev. Letters 17 (1966) 102.

23. D. V. Bugg, R. S. Gilmore, K. M. Knight, D. C. Salter, G. H. Stafford, E. J. N. Wilson, J. D. Davies, J. D. Dowell, P. M. Hattersley, R. J. Homer, A. W. O' Dell, A. A. Carter, R. J. Tapper, and K. F. Riley, Phys. Rev. 168 (1968) 1466.

24. R. Levi-Setti, Rapporteur Talk at the Lund International Conference on Elementary Particles, 1969.

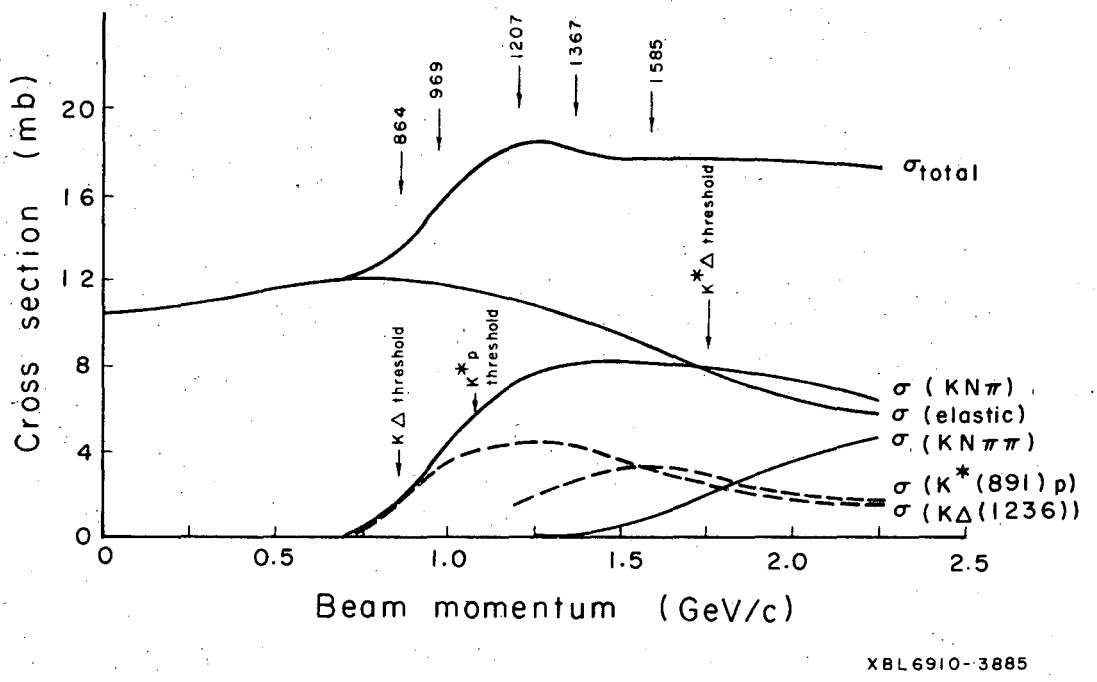
Cross section (mb)
20
16
12
8
4
0
0
0.5
1.0
1.5
2.0
2.5
Beam momentum (GeV/c)
864
969
1207
1367
1585
K*Δ threshold
K Δ threshold
K*p threshold
σ total
σ (KNπ)
σ (elastic)
σ (KNππ)
σ (K*(891) p)
σ (KΔ(1236))
XBL6910-3885

Fig. 1

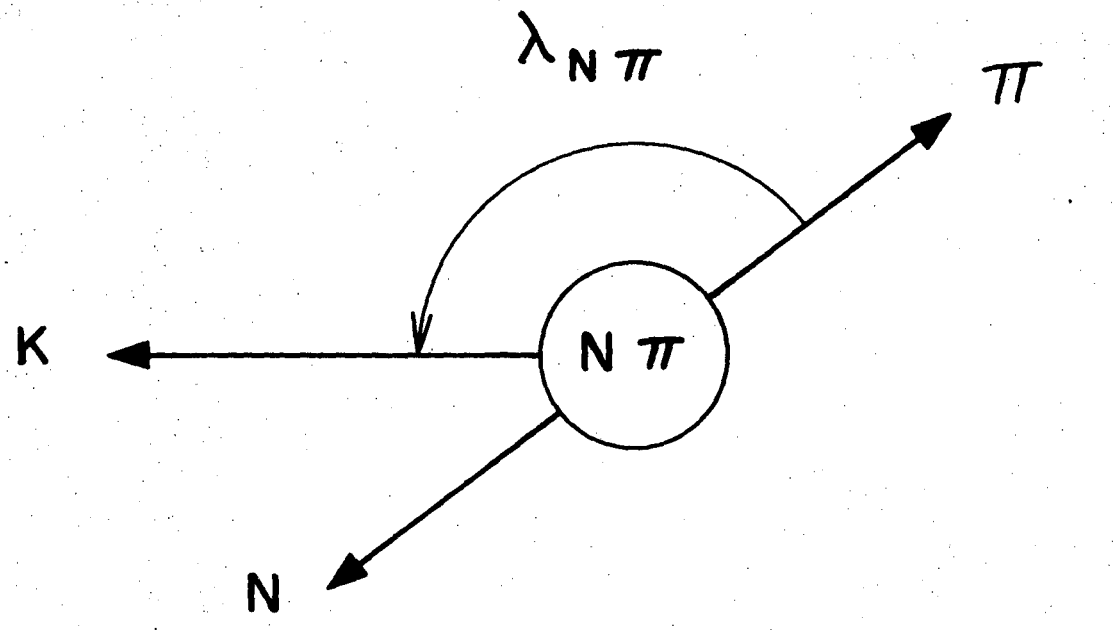

Fig. 2

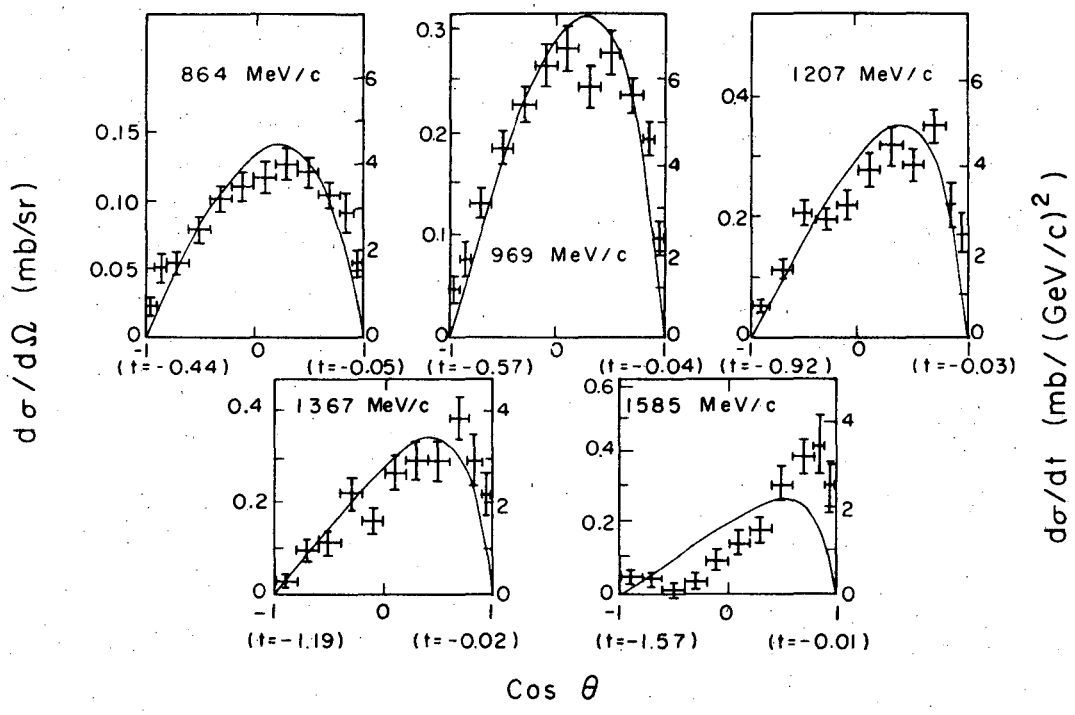
864 MeV/c
969 MeV/c
1207 MeV/c
1367 MeV/c
1585 MeV/c
(t=-0.44)
(t=-0.05)
(t=-0.57)
(t=-0.04)
(t=-0.92)
(t=-0.03)
(t=-1.19)
(t=-0.02)
(t=-1.57)
(t=-0.01)
dσ/dΩ (mb/sr)
dσ/dt (mb/(GeV/c)²)
Cos θ
XBL6910-3886

Fig. 3

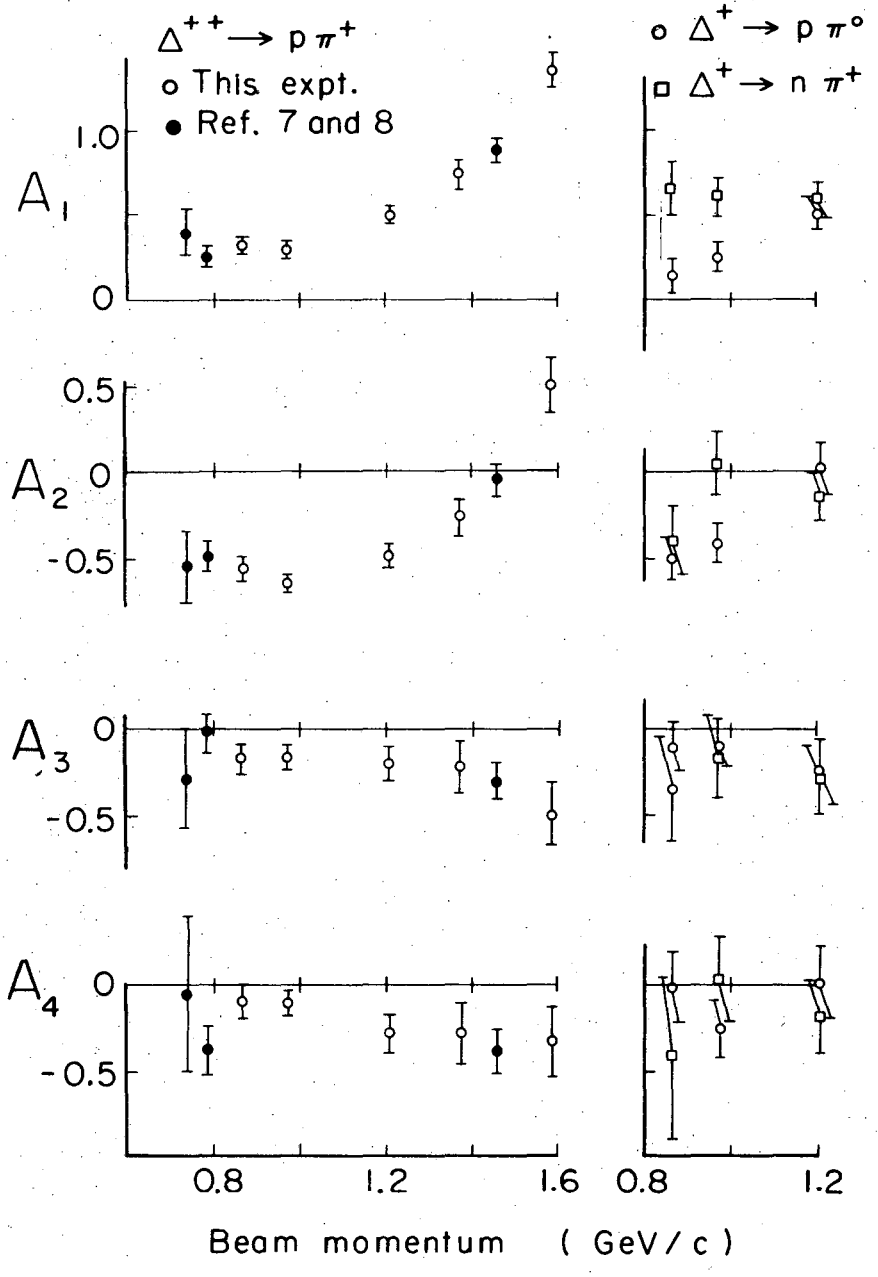
Δ++ → p π+
o This expt.
● Ref. 7 and 8
o Δ+ → p π°
□ Δ+ → n π+
A1
A2
A3
A4
1.0
0
0.5
-0.5
0.8
1.2
1.6
Beam momentum (GeV/c)
XBL6910-3887

Fig. 4

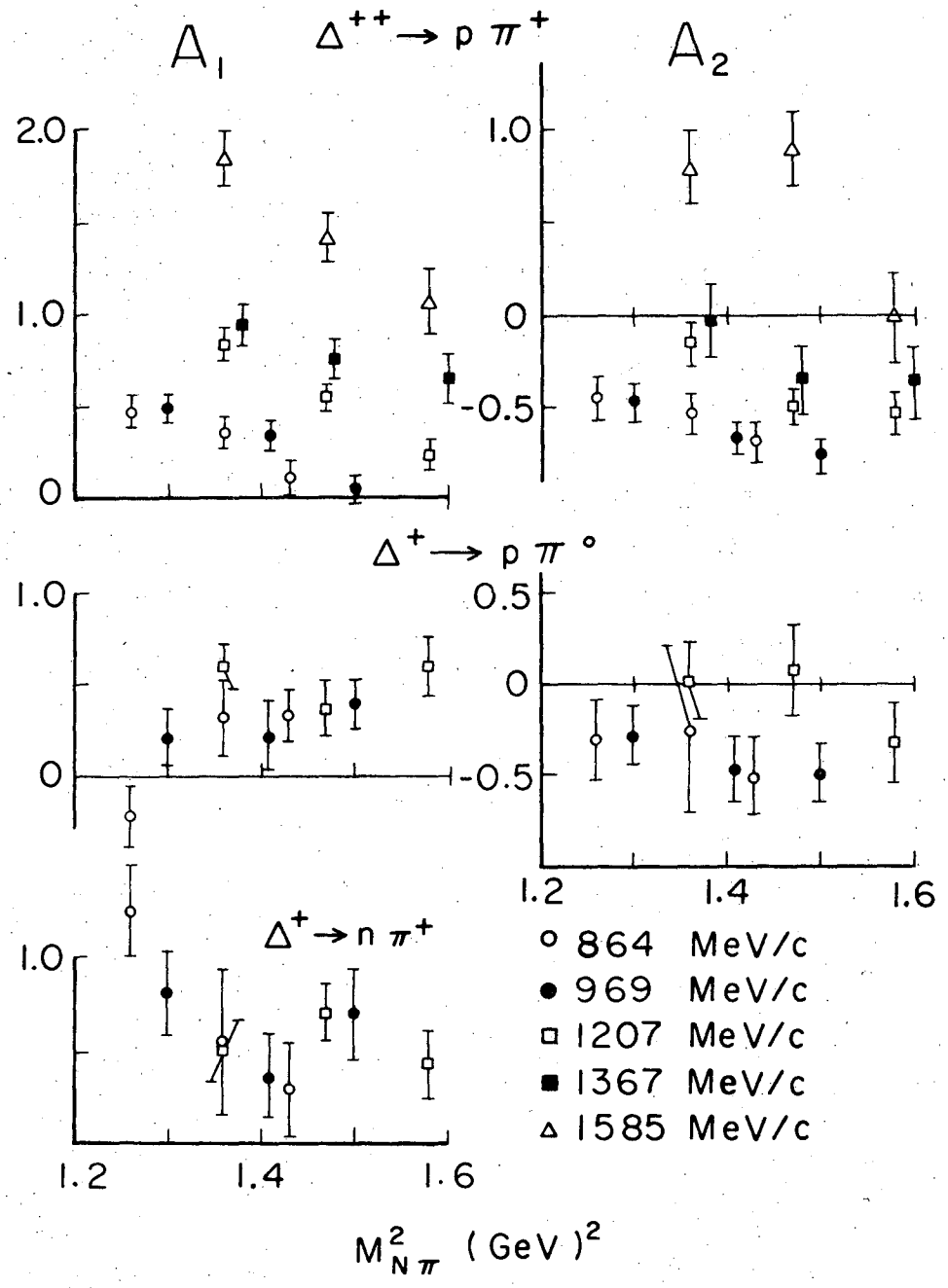
A1
Δ++ → p π+
A2
2.0
1.0
0
1.0
0
-0.5
Δ+ → p π °
1.0
0
0.5
0
-0.5
1.2
1.4
1.6
Δ+ → n π+
1.0
1.2
1.4
1.6
o 864 MeV/c
● 969 MeV/c
□ 1207 MeV/c
■ 1367 MeV/c
△ 1585 MeV/c
M2Nπ (GeV)2
XBL6910-3888

Fig. 5

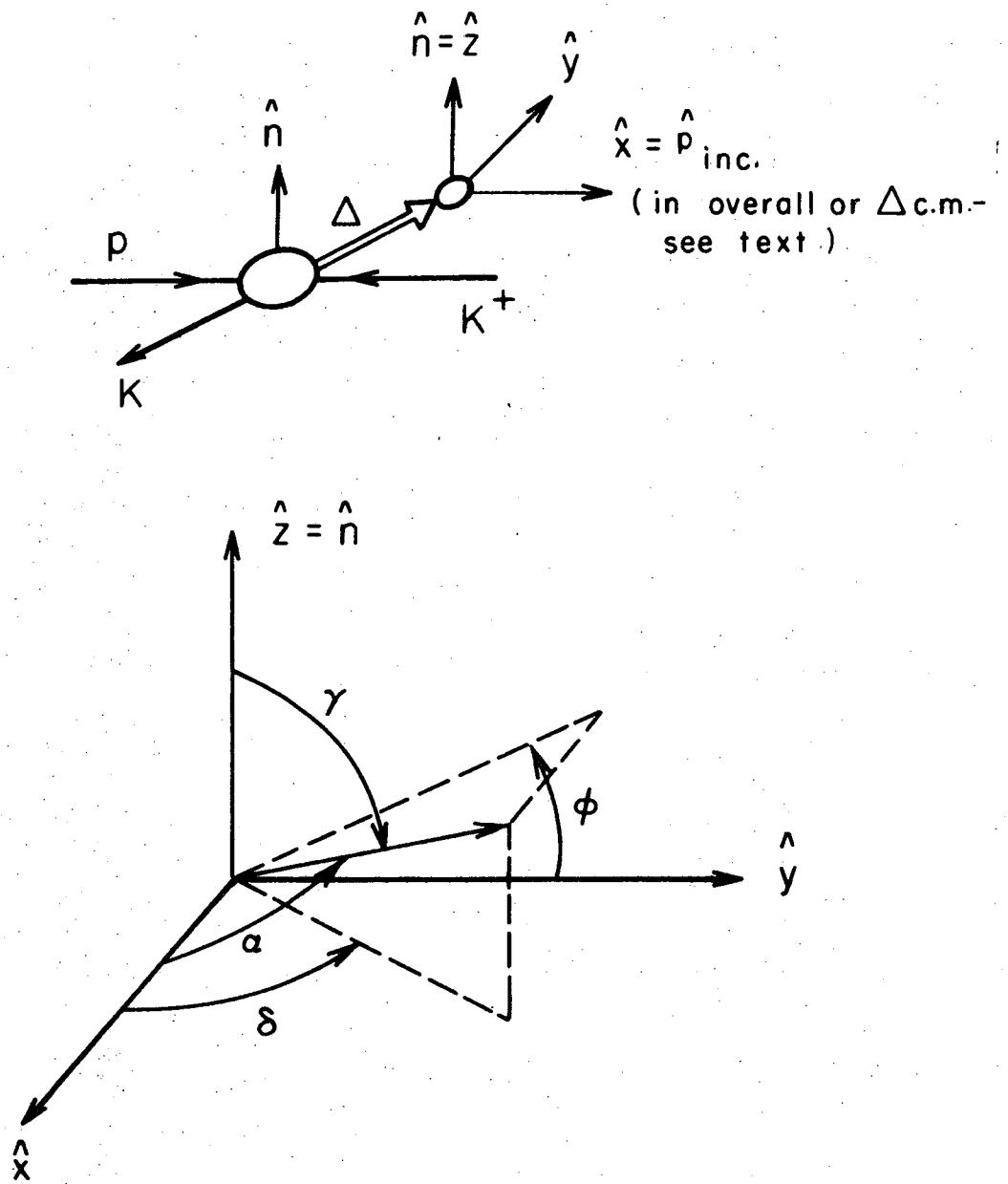
n̂ = ẑ
ŷ
n̂
x̂ = p̂ inc.
(in overall or Δ c.m.-
see text)
Δ
p
K+
K
ẑ = n̂
γ
φ
ŷ
α
δ
x̂
XBL6910-3889

Fig. 6

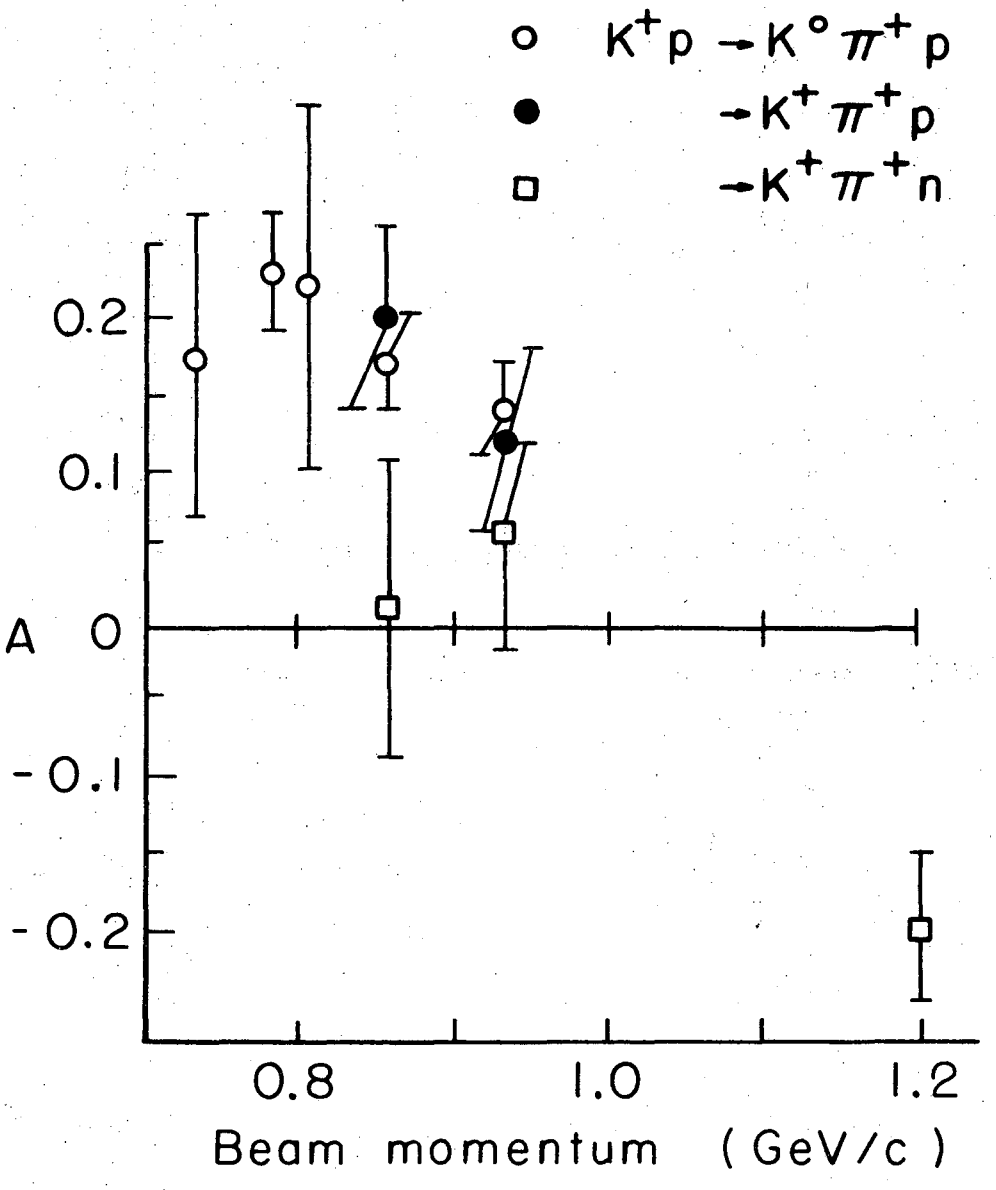

XBL6910-3890

Fig. 7

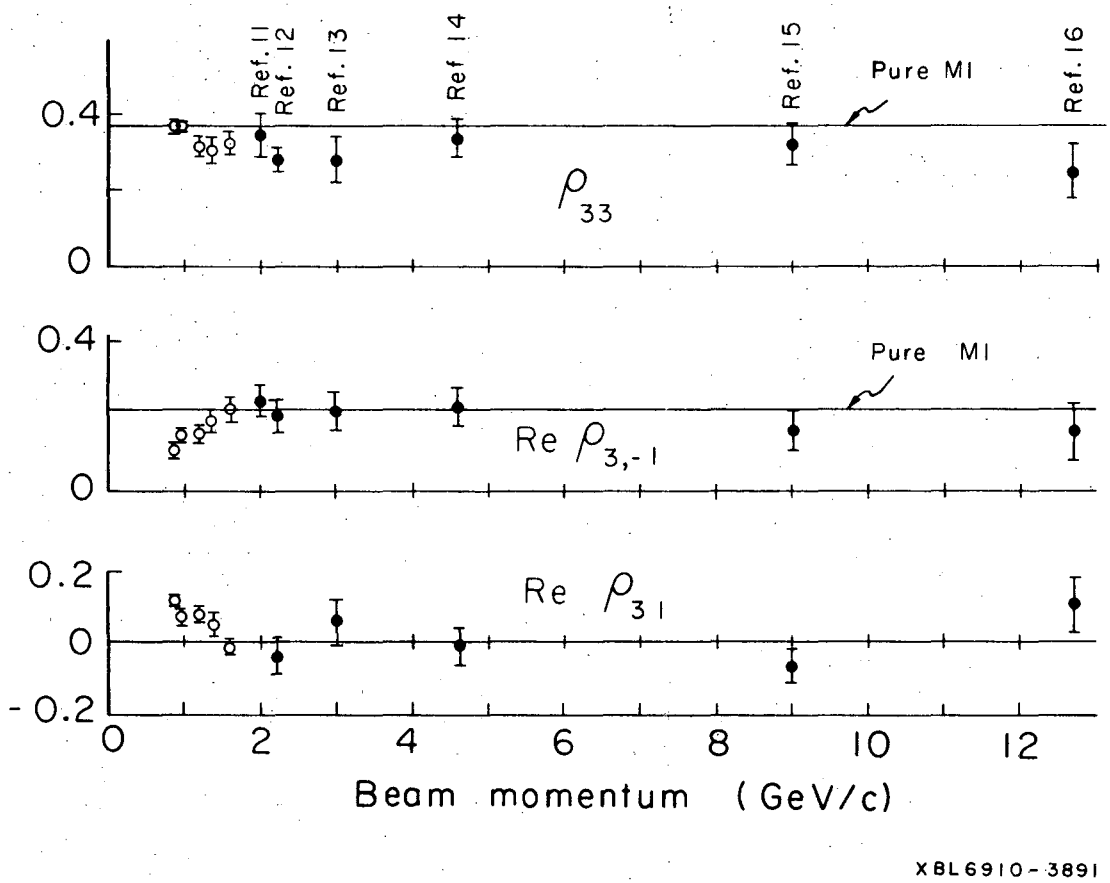
Ref. 11
Ref. 12
Ref. 13
Ref 14
Ref. 15
Pure MI
Ref. 16
0.4
0
ρ_{33}
0.4
0
Pure MI
Re $\rho_{3,-1}$
0.2
0
-0.2
Re ρ_{31}
0
2
4
6
8
10
12
Beam momentum (GeV/c)
XBL6910-3891

Fig. 8

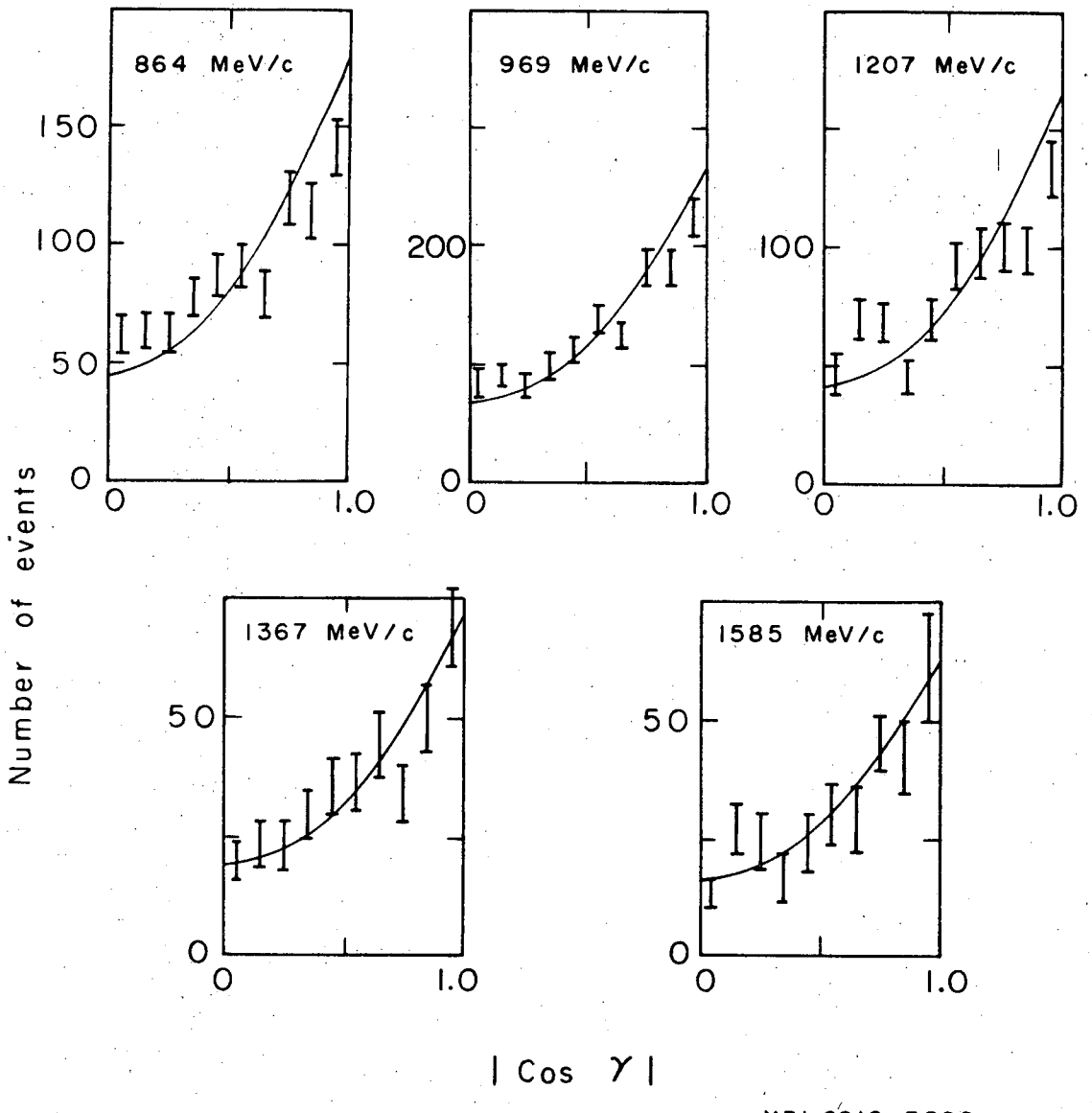
864 MeV/c
969 MeV/c
1207 MeV/c
1367 MeV/c
1585 MeV/c
Number of events
| Cos γ |
XBL6910-3892

Fig. 9

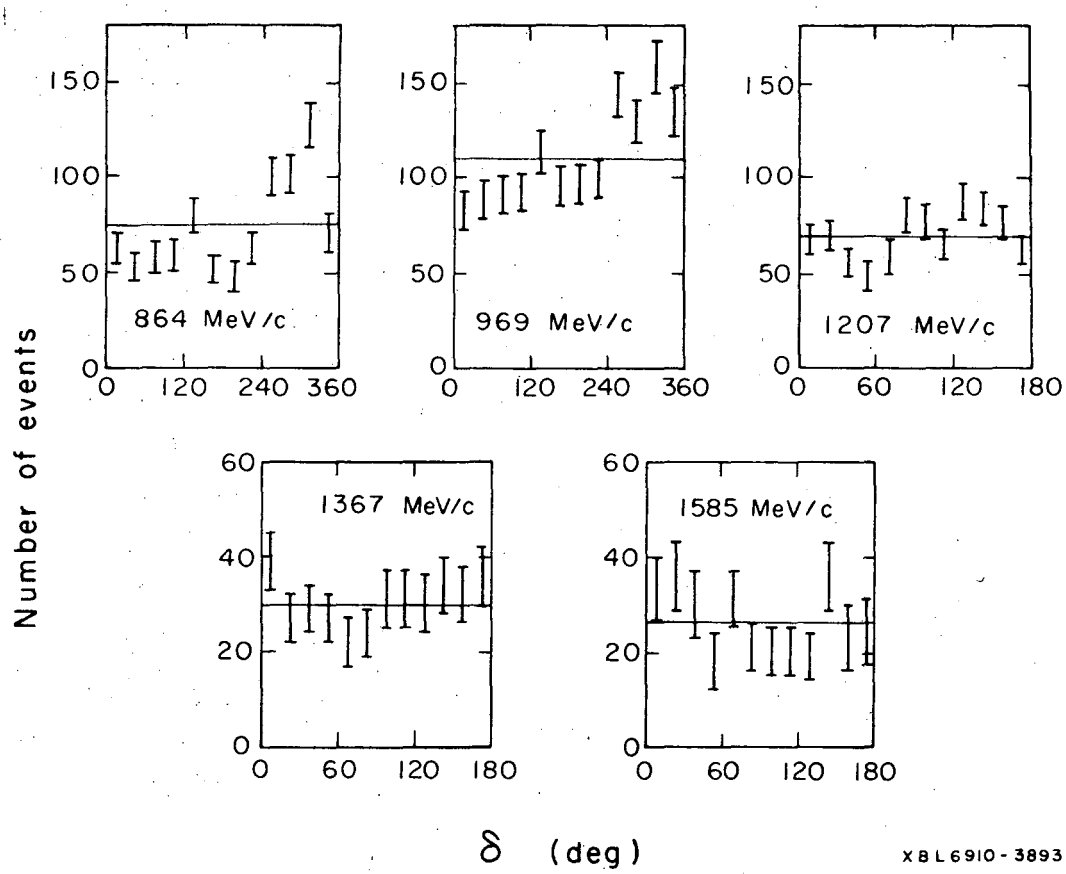
Number of events
150
100
50
0
0 120 240 360
864 MeV/c
969 MeV/c
0 60 120 180
1207 MeV/c
60
40
20
0
1367 MeV/c
1585 MeV/c
δ (deg)
XBL6910-3893

Fig. 10

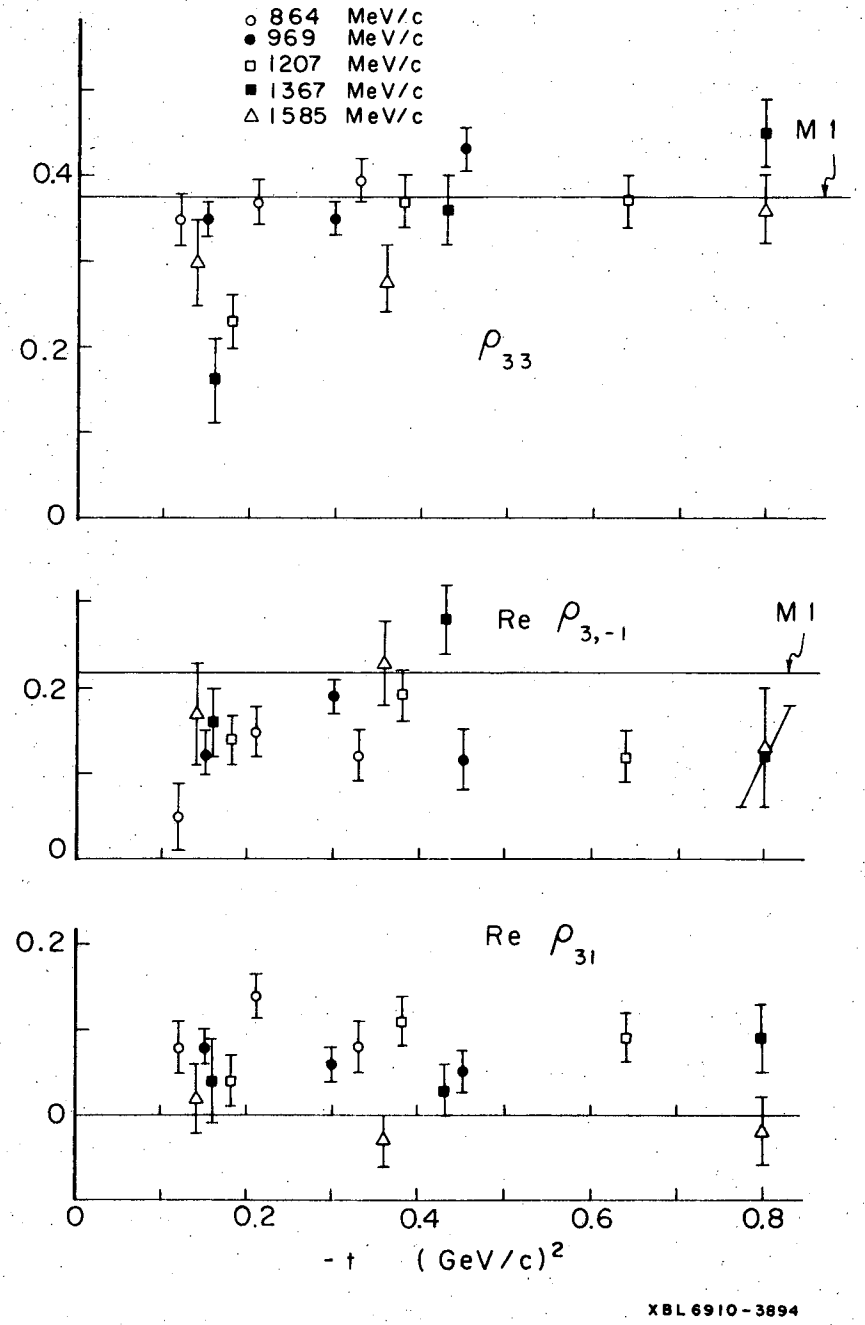
○ 864 MeV/c
● 969 MeV/c
□ 1207 MeV/c
■ 1367 MeV/c
△ 1585 MeV/c
M 1
0.4
0.2
0
ρ_{33}
Re $\rho_{3,-1}$
M 1
0.2
0
Re ρ_{31}
0.2
0
0
0.2
0.4
0.6
0.8
- t (GeV/c)^2
XBL 6910-3894

Fig. 11

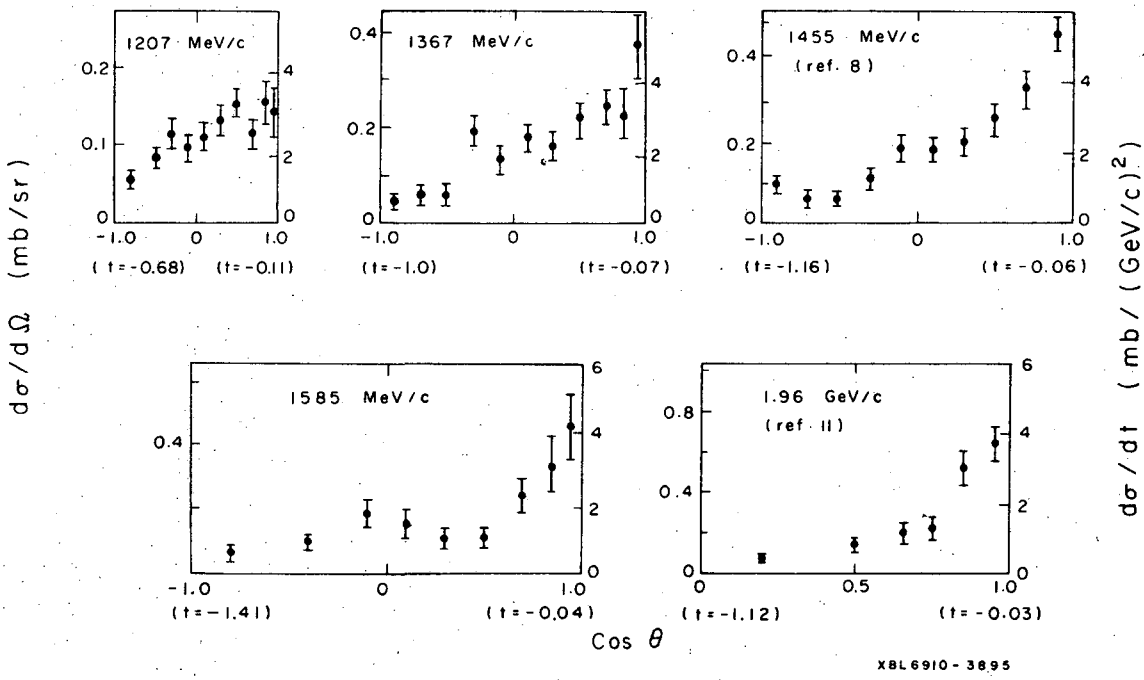
1207 MeV/c
1367 MeV/c
1455 MeV/c
(ref. 8)
1585 MeV/c
1.96 GeV/c
(ref. 11)
(t=-0.68)
(t=-0.11)
(t=-1.0)
(t=-0.07)
(t=-1.16)
(t=-0.06)
(t=-1.41)
(t=-0.04)
(t=-1.12)
(t=-0.03)
dσ/dΩ (mb/sr)
dσ/dt (mb/(GeV/c)²)
Cos θ
XBL6910-3895

Fig. 12

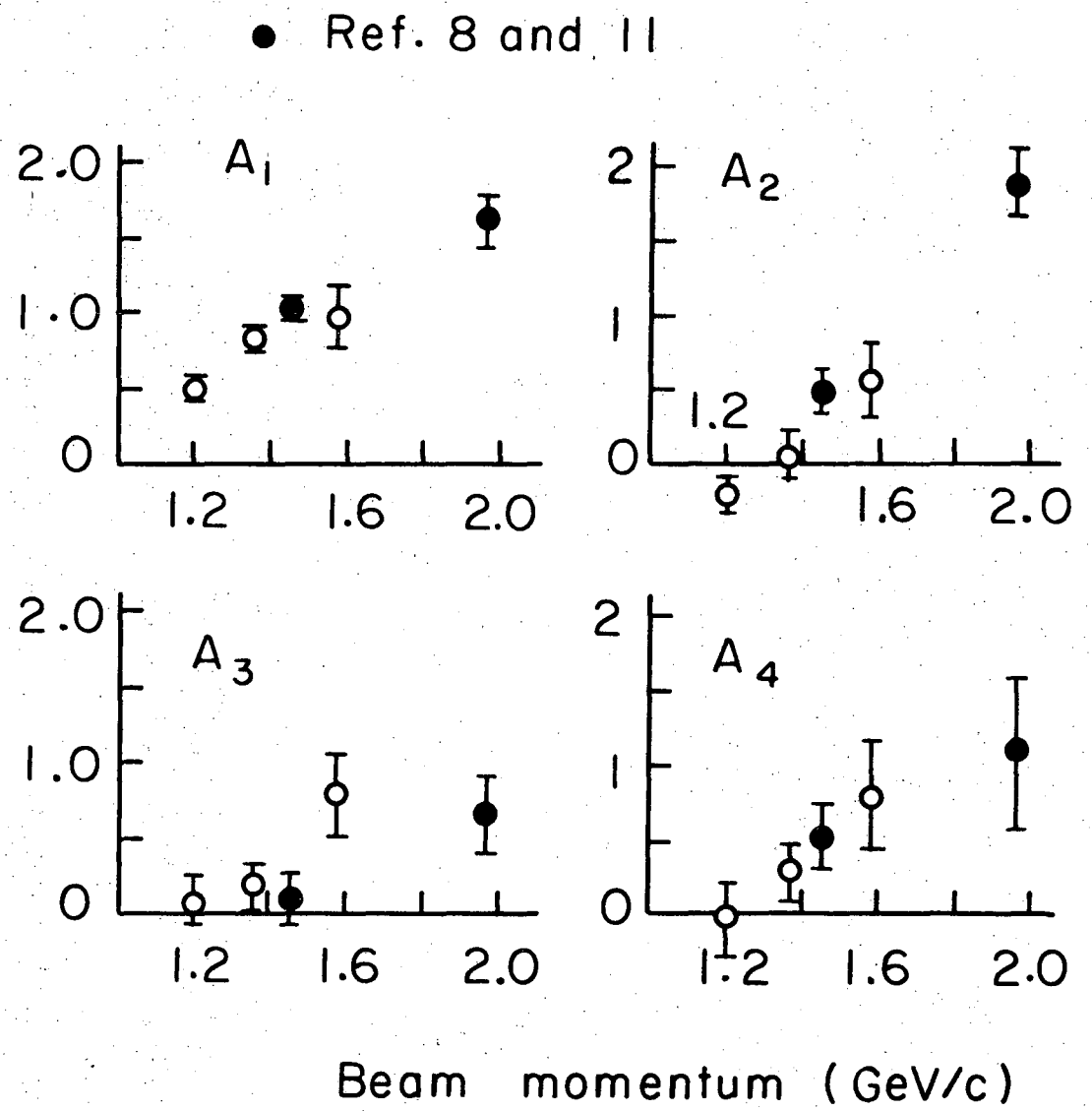
● Ref. 8 and 11
A1
A2
A3
A4
2.0
1.0
0
2
1
1.2
1.6
2.0
Beam momentum (GeV/c)
XBL6910-3898

Fig. 13

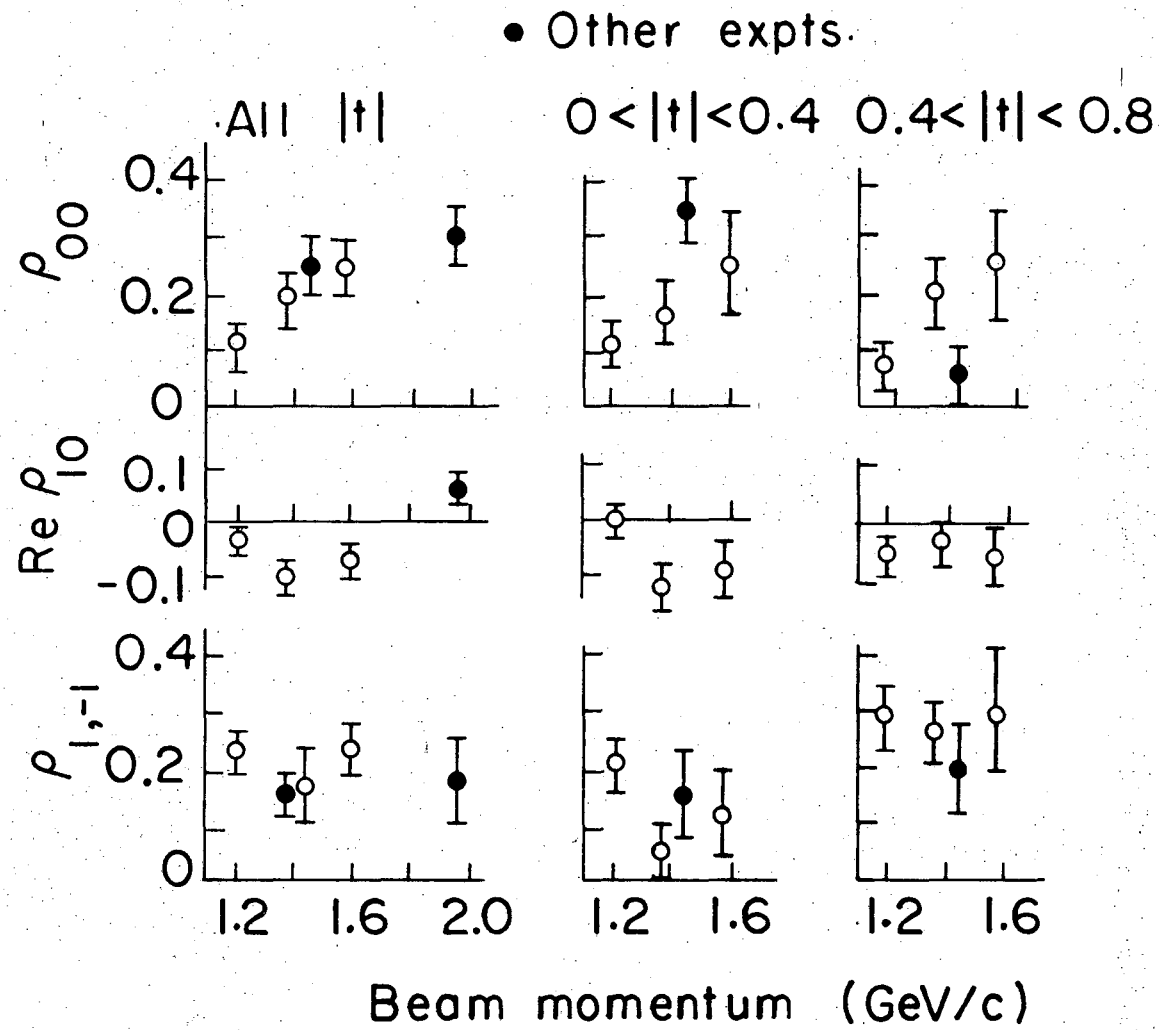

XBL6911-3899

Fig. 14

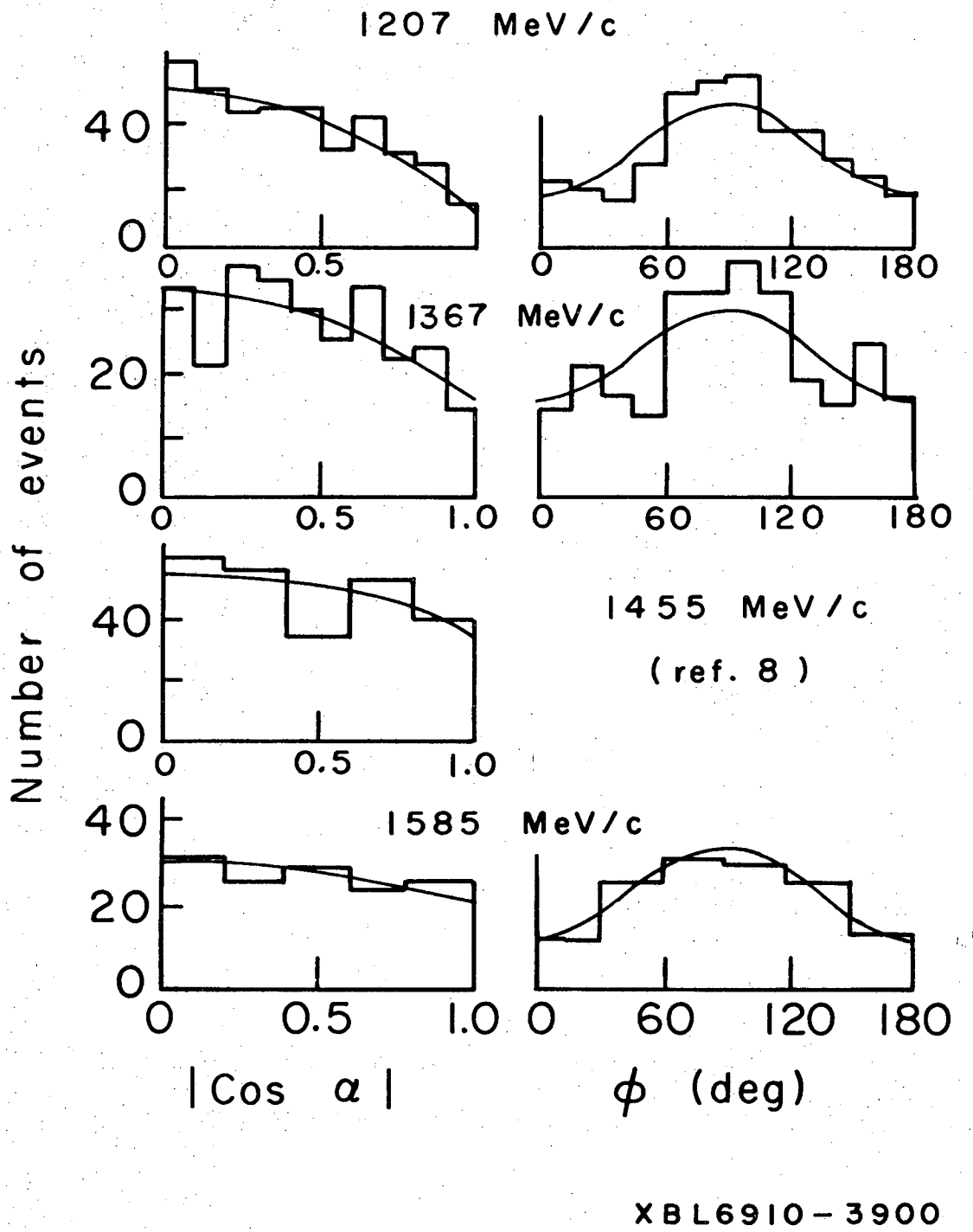
1207 MeV/c
1367 MeV/c
1455 MeV/c
(ref. 8)
1585 MeV/c
Number of events
40
20
0
0.5
1.0
60
120
180
|Cos α|
φ (deg)
XBL6910-3900

Fig. 15

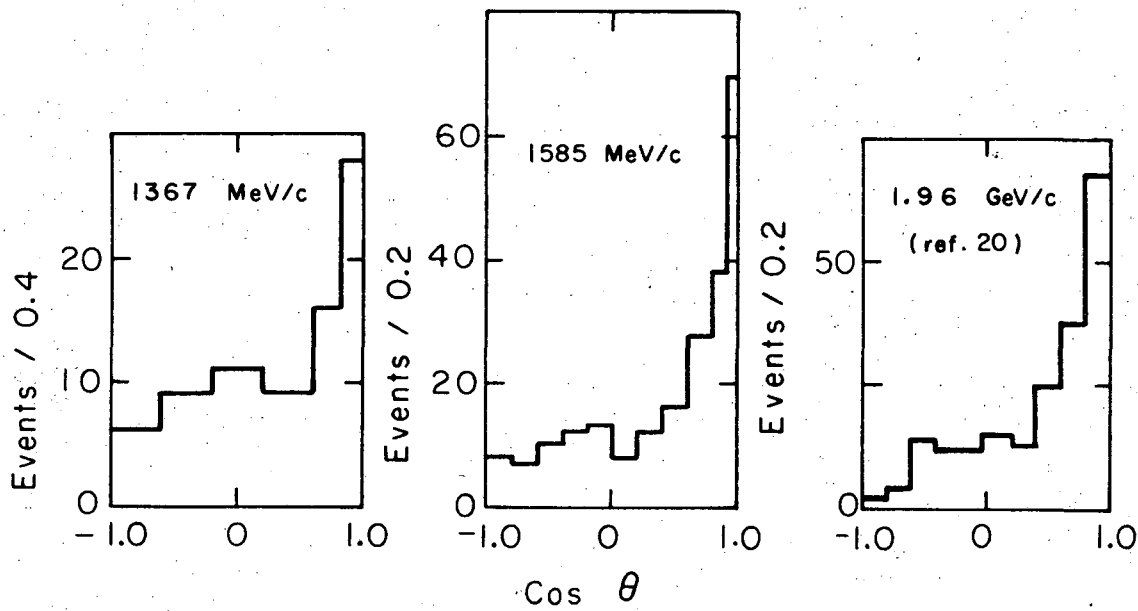
1367 MeV/c
1585 MeV/c
1.96 GeV/c
(ref. 20)
Events / 0.4
Events / 0.2
Events / 0.2
Cos θ
XBL6910-3906

Fig. 16

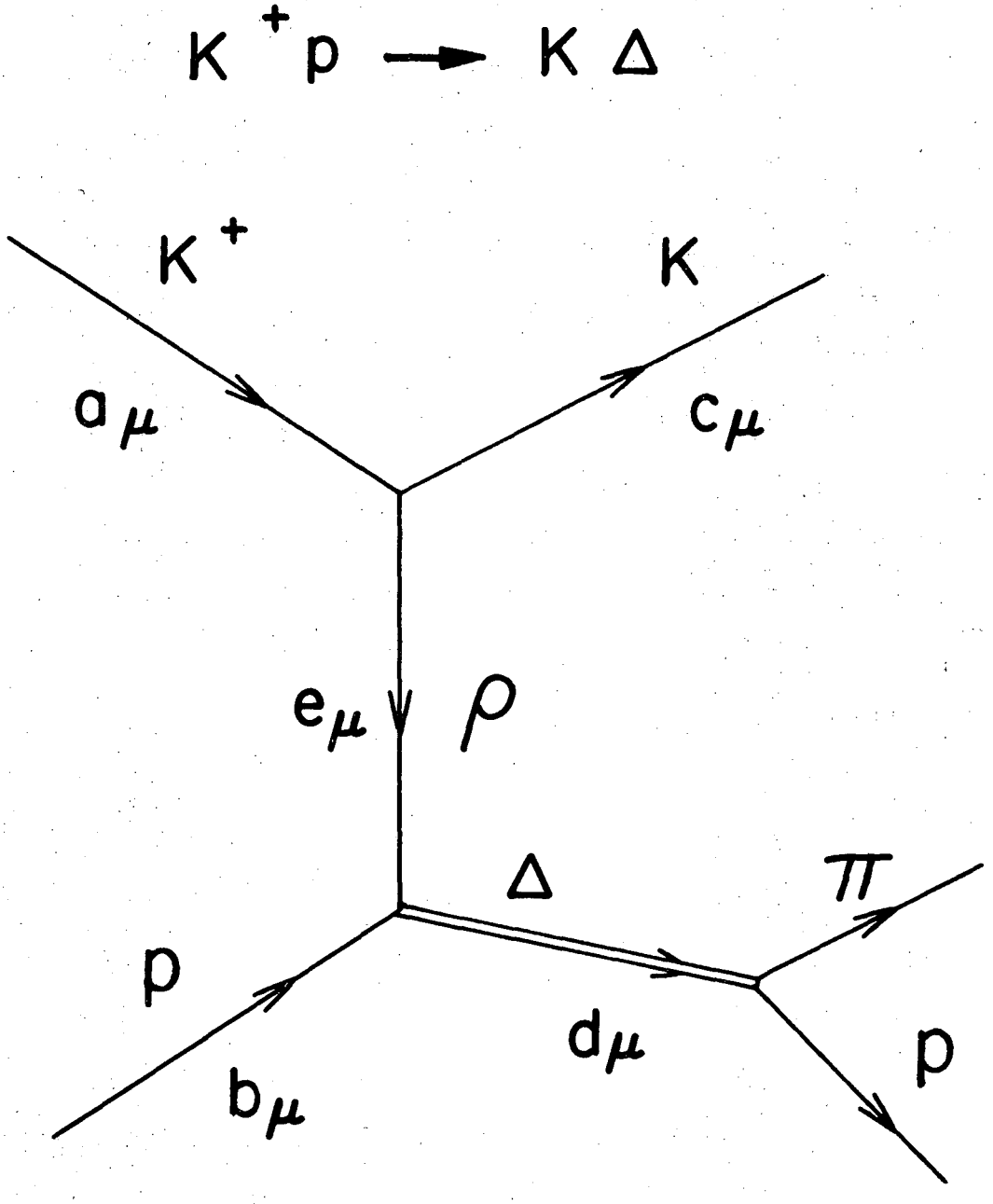

Fig. 17

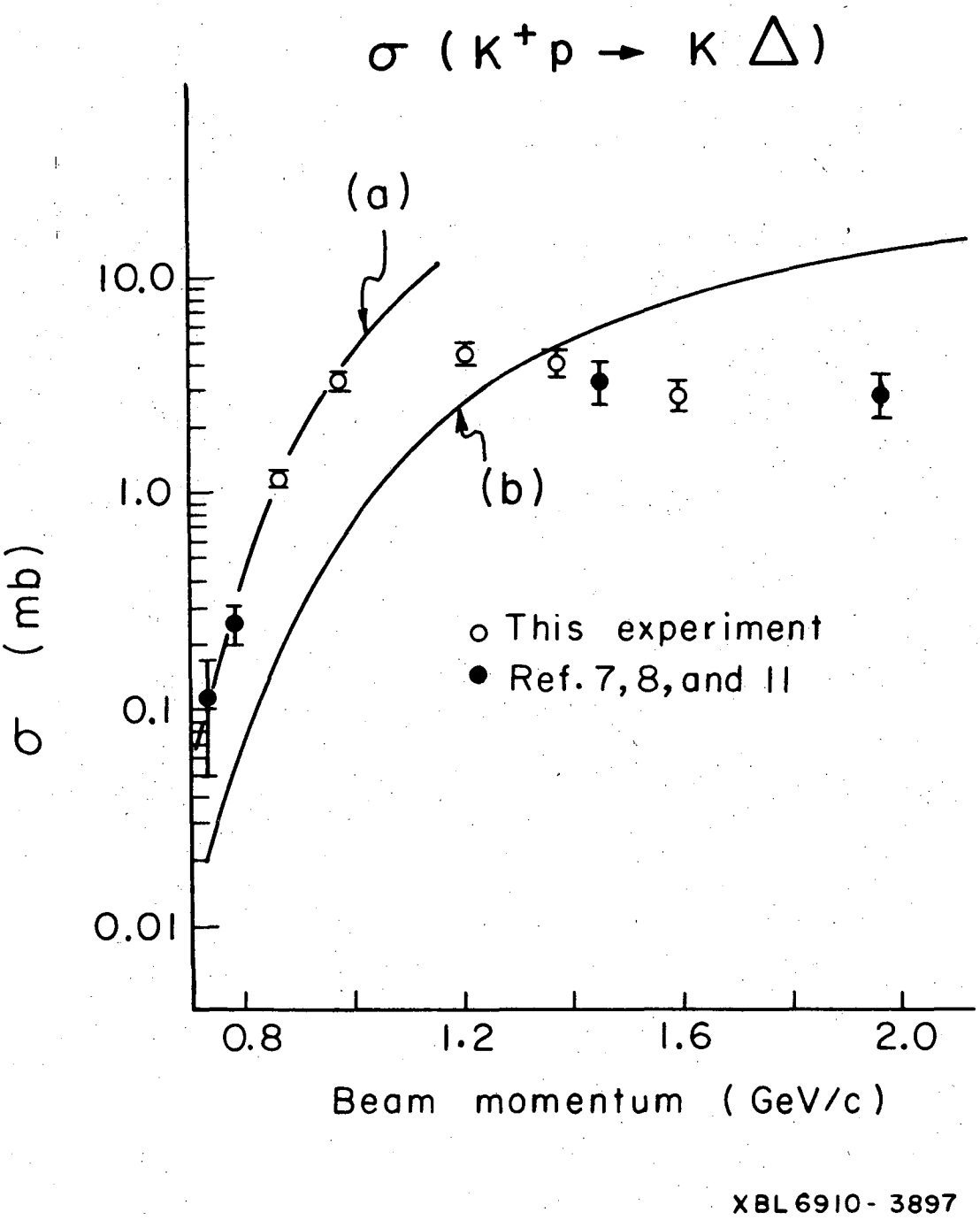
σ (K⁺p → K Δ)
(a)
(b)
10.0
1.0
0.1
0.01
σ (mb)
o This experiment
● Ref. 7, 8, and 11
0.8
1.2
1.6
2.0
Beam momentum (GeV/c)
XBL6910-3897

Fig. 18

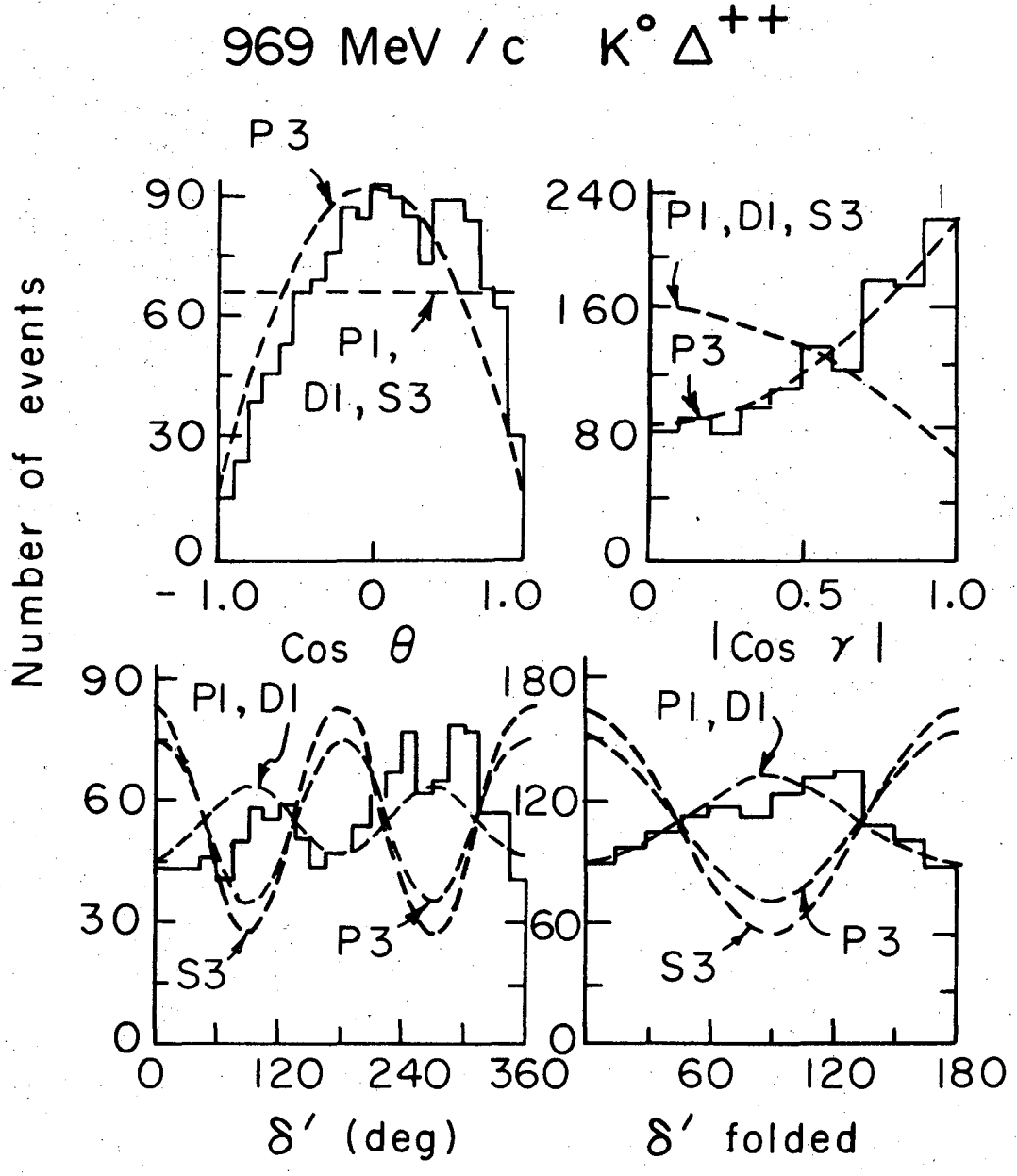
969 MeV / c K° Δ++
P 3
P1, D1, S3
P1, D1, S3
P3
Number of events
Cos θ
|Cos γ|
P1, D1
P3
S3
δ′ (deg)
δ′ folded
XBL 6910-3896

Fig. 19

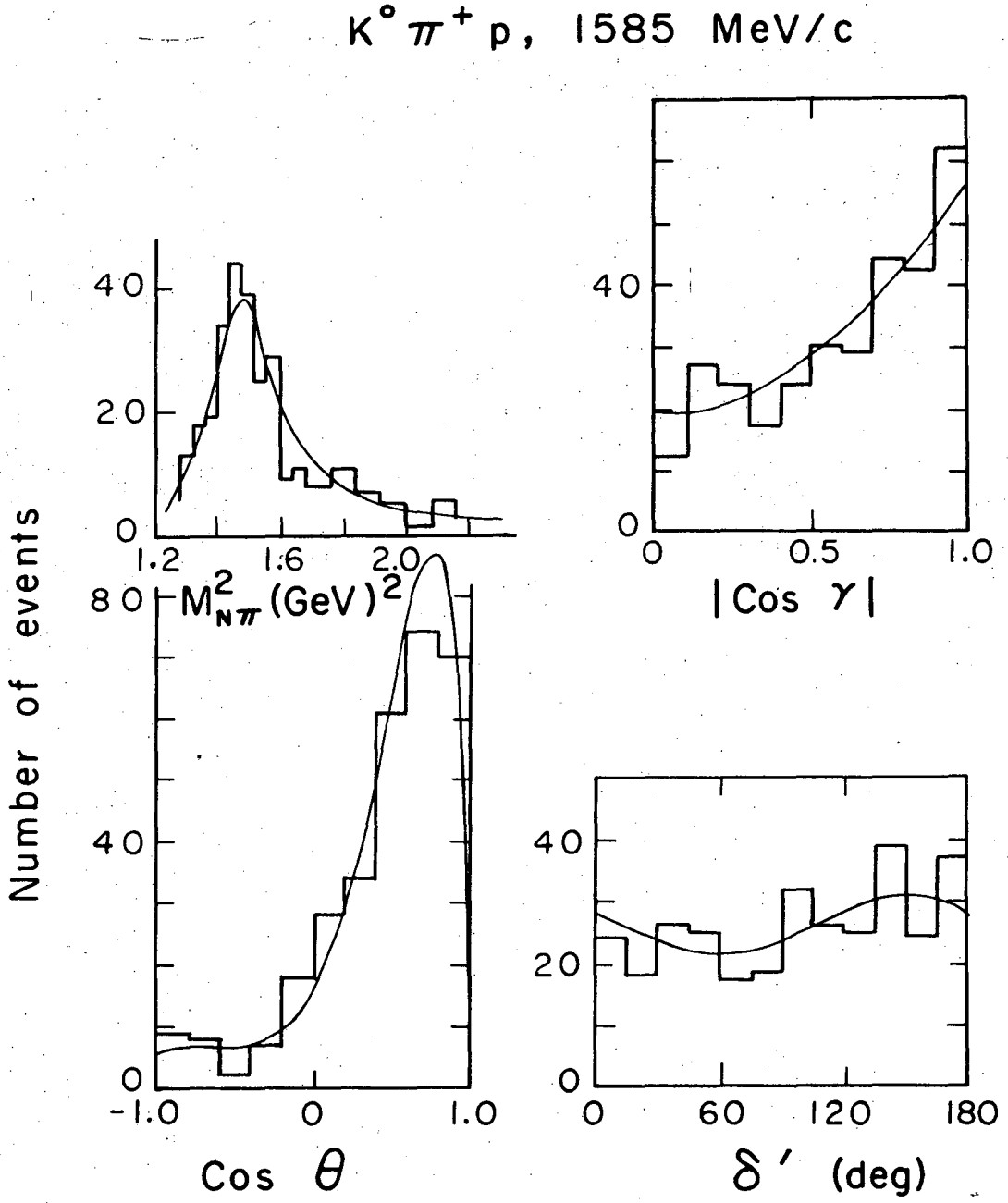
K° π⁺ p, 1585 MeV/c
Number of events
40
20
0
1.2
1.6
2.0
$M^2_{N\pi}$ (GeV)^2
40
0
0.5
1.0
|Cos γ|
80
40
0
-1.0
0
1.0
Cos θ
40
20
0
0
60
120
180
δ′ (deg)
XBL6910-3905

Fig. 20

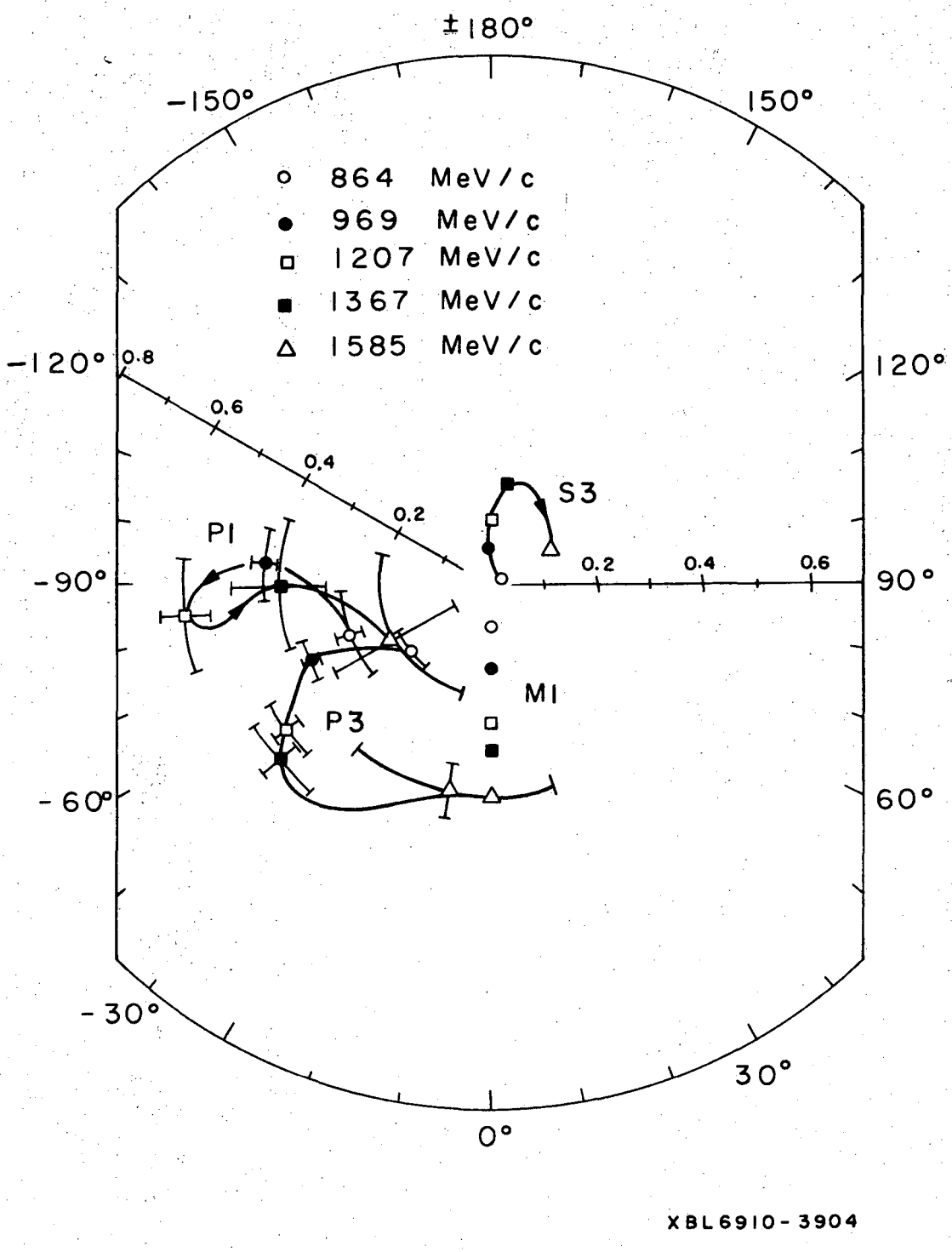
±180°
-150°
150°
-120°
120°
-90°
90°
-60°
60°
-30°
30°
0°
0.8
0.6
0.4
0.2
0.2
0.4
0.6
864 MeV/c
969 MeV/c
1207 MeV/c
1367 MeV/c
1585 MeV/c
P1
S3
M1
P3
XBL6910-3904

Fig. 21

TECHNICAL INFORMATION DIVISION
LAWRENCE RADIATION LABORATORY
UNIVERSITY OF CALIFORNIA
BERKELEY, CALIFORNIA 94720